

Science Requirements Document

Version 1.0

25 Dec, 2012

For

Residence Time Driven Flame Spread Over Solid Fuels

Principal Investigator:

Subrata Bhattacharjee
subrata@thermo.sdsu.edu
San Diego State University
San Diego, CA 92182

Co-Investigator:

Christopher Paolini
Fletcher Miller
San Diego State University
San Diego, CA 92182

Kazunori Wakai
Shuhei Takashashi
Gifu University, Japan

Project Scientist:

Paul Ferkul, NASA GRC

EXECUTIVE SUMMARY

The proposed space based work builds upon our ground based studies - theoretical, computational and experimental – and earlier space based experiments to investigate steady and unsteady flame propagation over solid fuels in a microgravity environment. Our theoretical work based on scale modeling predicts that steady flame spread over solid fuels cannot be sustained even at high oxygen environment if the fuel is thicker than a critical thickness. Flame spread rate over thin fuels in a quiescent microgravity environment decreases with fuel thickness not only because of increased thermal mass but also because the relative importance of radiative losses, as quantified by a non-dimensional radiation number, increases in direct proportion of fuel thickness. A comprehensive computational model that includes gas and surface radiation, finite-rate chemistry for pyrolysis and combustion has been validated by comparing its prediction for downward spreading flames over fuels of different thicknesses with experiments. Not only the spread rate is predicted with sufficient accuracy, but the flame shape and thermal signature of a spreading flame also compare well with experimental results. This model, applied to the quiescent microgravity regime, also predicts flame extinguishment even in a pure oxygen environment for sufficiently thick fuels. Moreover, computations reveal that the asymmetry between the thermal and species fields introduced by radiative losses is responsible for a slowly moving flame to be surrounded by a vitiated atmosphere leading to extinguishment. Earlier space based experiments showed a slowing flame over thick PMMA slabs consistent with our findings. Sufficient microgravity time is necessary to test our hypothesis that a critical fuel thickness exists below which flame can spread steadily and above which the flame slows down leading to extinguishment.

The non-dimensional radiation number being proportional to fuel thickness and inversely proportional to the ambient pressure, we propose to vary these two parameters in long duration experiments in the International Space Station (ISS). The intended experiments will provide direct evidence to prove or disprove our prediction of flame extinguishment and give us unprecedented insight into the mechanism of flame spread in a microgravity environment. Our project goals include determination of instantaneous flame spread rate over PMMA sheets of various thicknesses under different ambient pressures and comparison with theory and computational predictions. Additionally, measurement of gas field temperature and CO₂ concentrations at a number of locations will provide valuable data for comparison with modeling results. A thoroughly validated model then can be used for predicting presence or absence of steadily spreading flame over different fuels under different ambient conditions with implications of developing computational tools to predict fire safety of different materials in a microgravity environment.

1. INTRODUCTION

Flame spread over solid fuels in an opposed-flow environment has been investigated for over four decades for understanding the fundamental nature of hazardous fire spread. The appeal for this configuration stems from the fact that flame spread rate remains steady even if the flame itself may grow in size. For practical fire safety issues on earth, however, concurrent-flow or wind-assisted flame spread is more relevant. Although there is a good amount of literature on both of these configurations, a connection between the two regimes is yet to be established. The microgravity regime can be thought to be sitting between these two regimes, where the oxidizer flow can be mild or even completely absent, drastically increasing the residence time of the oxidizer flow.

It has been established through numerical research [1,2,3] that in the high residence time environment of microgravity, radiation plays a dominant role in the transport of energy. In the SSCE [4] project, flame spread over thick PMMA samples could not be sustained in a quiescent environment even at relatively high oxygen levels (70% oxygen in an oxygen/nitrogen mixture). A computational model [5] indicated that radiative losses from the flame create a mismatch between the temperature and the species fields. Embedded in a vitiated atmosphere of its own creation, the flame extinguishes inherently. For thin cellulosic fuels, however, the flame was found to spread vigorously in the same environment [4]. This suggests that the thickness of the fuel plays an important role in the extinction process in a microgravity environment. Based on a numerical solution of a theoretical model that included surface radiation, T'ien [6] proposed a radiative quenching branch for thin fuels. For a flow velocity below a numerically calculated critical velocity, no steady spread rate could be calculated. The same trend was confirmed by Olson et al. [7] in their drop-tower experiments with thin cellulosic fuels. However, a general quantitative criterion is yet to be established. In the ground based research [8], scaling arguments and a numerical model was used to develop flame closed-form spread formulas in a microgravity environment that included the effect of surface radiation through a non-dimensional radiation parameter. The results indicated that a critical thickness of fuel exists, above which a fuel is self-extinguishing under any environmental condition in a quiescent environment. The formulas developed in that research remains to be verified through space based experiments.

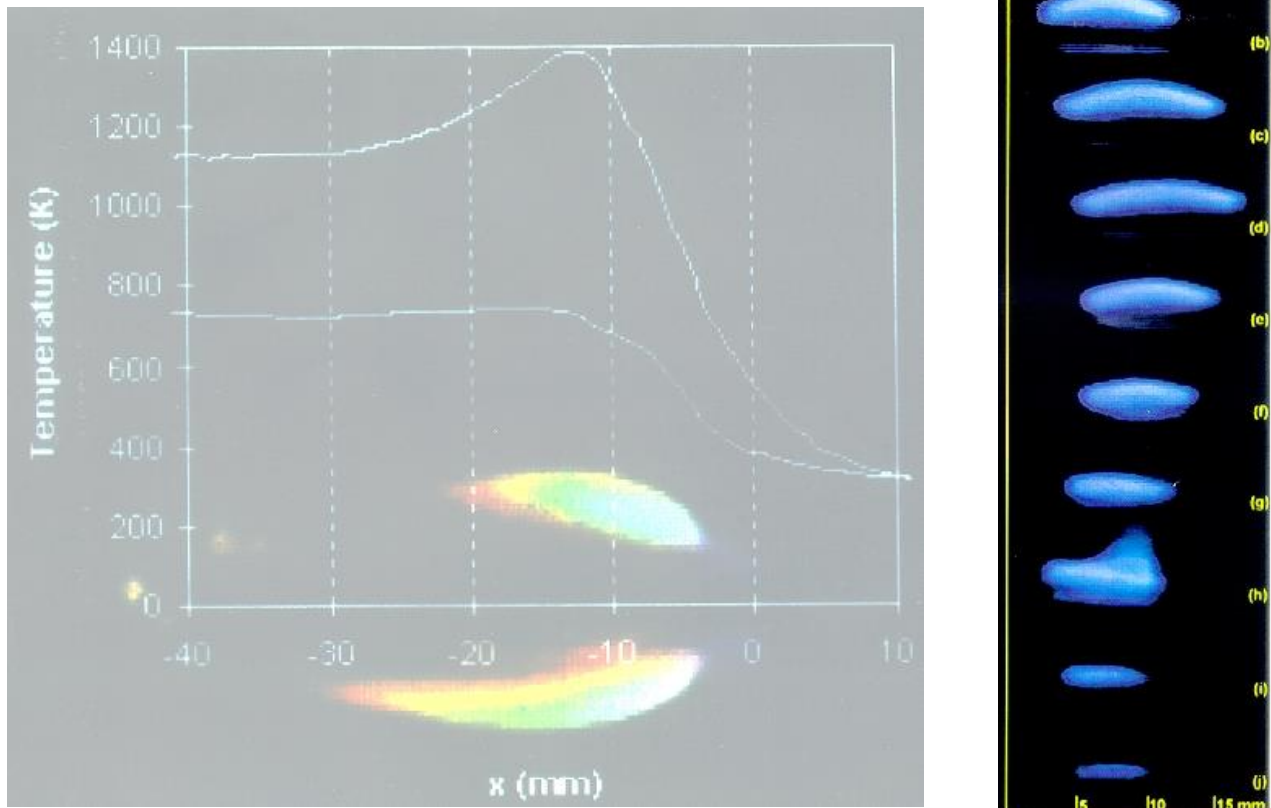


Fig. 1 SSCE [4] experiments showed that flame spreads steadily over thin ashless filter paper but gradually slows down when spreading over thick PMMA slab.

2. GROUND BASED EFFORT

2.1 Scale Modeling of Microgravity Flame Spread

Scaling arguments leads to the conclusion that the dominance of radiation in the microgravity regime stems from the increased residence time – the ratio of the characteristic length of the flame to the characteristic oxidizer velocity – due to small velocity scale. In terrestrial flames, however, the induced flow due to buoyancy reduces the residence time for small flames (as encountered in opposed-flow flame spread) and there is not sufficient time for the radiative transport to become significant compared to advection. Therefore, radiative effects are observed only in large fires, where the residence time goes up due to the increased flame height.

We start with the opposed-flow configuration shown in 2 - a configuration with demonstrably [9] higher potential of fire hazard in a semi-quiet environment of microgravity

- which depicts a laminar flame propagating over a solid fuel in the flame fixed coordinates. The opposing flow velocity V_g , in general, can be due to forced-flow or flow induced from the residual gravity in a microgravity environment. With respect to the flame, the oxidizer, assumed to be a mixture of oxygen and nitrogen, approaches with a velocity $V_r = V_g + V_f$ and the fuel with a velocity V_f . Notice that even in a perfectly quiescent environment, V_f itself provides the opposing velocity in the flame-fixed coordinates. For that matter, the opposed-flow flame spread configuration applies as long as $V_g < V_f$.

To identify the relevant time and length scales, we focus our attention on the leading edge of the flame, sketched in Fig. 2, where forward heat transfer to the virgin fuel, the fundamental mechanism of any flame spread [10], takes place. Two control volumes, one in the gas phase of size $L_{gx} \times L_{gy} \times W$ and one in the solid phase of size $L_{sx} \times L_{sy} \times W$, are drawn at the flame leading edge, W being the fuel-width in the z direction and the length scales, L_{gx} , L_{gy} , L_{sx} and L_{sy} , unknown at this point.

In the gas-phase control volume the vaporized fuel and oxidizer react to raise the gas temperature from its ambient value T_∞ to a characteristic flame temperature T_f . In these flame-fixed coordinates, the velocity at which the solid fuel must be fed through the solid-phase control volume in the x direction to steadily raise the fuel temperature, from its ambient value of T_∞ to a characteristic vaporization temperature T_v is the desired spread rate V_f .

There are two characteristic residence times at the leading edge,

$$t_{res,g} \sim \frac{L_{gx}}{V_r} \text{ in the gas phase and}$$

$$t_{res,s} \sim \frac{L_{sx}}{V_f} \text{ in the solid. Even in the}$$

absence of forced opposing flow,

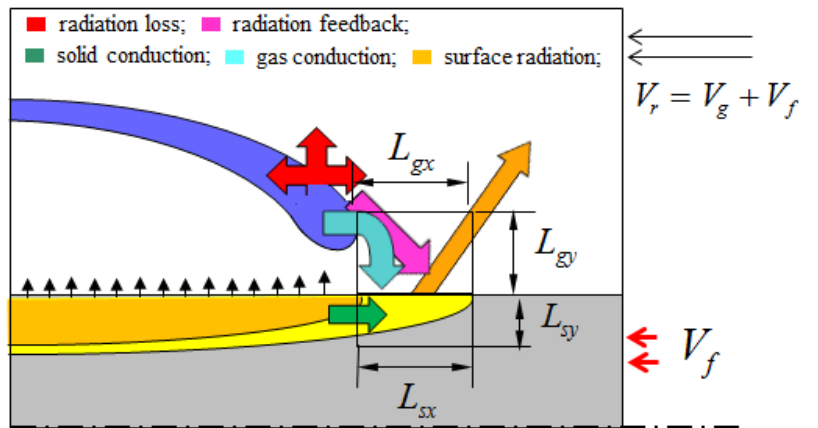


Fig. 2 Length scales at the leading edge of the flame in the flame-fixed coordinates.

buoyancy at normal gravity ensures that $V_g \gg V_f$. The thermal regime of flame spread is based on a few simplifying assumptions. The ambient conditions are so chosen as to render $t_{res,g}$ large compared to the characteristic chemical time t_{chem} so that gas-phase can be treated as infinitely fast. At the same time $t_{res,g}$ is assumed small compared to the radiative time scales, justifying the neglect of all radiative effects, an issue that will be discussed in more detail in latter sections. The adiabatic flame temperature, therefore, can be used as the characteristic flame temperature. In the solid phase, the characteristic vaporization time t_{vap} is assumed small compared to $t_{res,s}$ allowing the use of a constant vaporization temperature. The spread mechanism, therefore, is completely heat transfer limited and the resulting regime is known as the thermal regime [11].

2.1.1 Length Scales: In the gas-phase, a balance between conduction and convection in the x -direction at the leading edge yields the familiar [10,12] expression for L_{gx} , while L_{gy} can be obtained following Delichatsios [13,14] as the diffusion length in the y -direction within the available residence time.

$$L_{gx} \sim \frac{\alpha_g}{V_r}; \quad L_{gy} \sim \sqrt{\alpha_g t_{res,g}} = \frac{\alpha_g}{V_r} = L_{gx}; \quad \text{Therefore, } L_g \equiv L_{gx} = L_{gy} \quad (1)$$

The gas-phase conduction being the driving force under all but extreme situations [15], L_g is imposed on the solid phase making $L_{sx} \sim L_g$. The transverse length L_{sy} , for a semi-infinite fuel bed can be derived in a similar manner.

$$L_{sy} \sim \sqrt{\alpha_s t_{res,s}} \sim \sqrt{\alpha_s \frac{L_{sx}}{V_f}} \sim \sqrt{\frac{\alpha_s \alpha_g}{V_f V_r}}. \quad (2)$$

A fuel with a half-thickness of $\tau < L_{sy}$ must be heated uniformly throughout across its thickness and is, therefore, considered thermally thin. To generalize the expression for the thickness of the heated layer, we introduce τ_h , define as:

$$\tau_h \sim \min[\tau, L_{sy}] \sim \min\left[\tau, \sqrt{\frac{\alpha_s \alpha_g}{V_f V_r}}\right]. \quad (3)$$

Note that the spread rate is still an unknown in these expressions.

2.1.2 Spread Rate Formulas in the Thermal Regime: An energy balance for the solid phase control volume of Fig. 2 yields the spread rate.

$$\lambda_g \frac{(T_f - T_v)}{L_{gy}} L_{gx} W \sim V_{f,thermal} \rho_s c_s \tau_h W (T_v - T_\infty) \quad (4)$$

Hence, $V_{f,thermal} \sim \frac{\lambda_g}{\rho_s c_s \tau_h} F$, where F is the flame constant defined as $F \equiv \frac{T_f - T_v}{T_v - T_\infty}$ (5)

The thin and thick limits of τ_h from Eq. (3), when substituted into Eq. (5), produce:

$$V_{f,thermal,thin} \sim \frac{\lambda_g}{\rho_s c_s \tau} F \quad \text{and} \quad V_{f,thermal,thick} \sim V_r \frac{\lambda_g \rho_g c_g}{\lambda_s \rho_s c_s} F^2. \quad (6)$$

These expressions are identical (except for a constant $\pi/4$ for thin fuel) to the analytical solutions of de Ris [16] and Delichatsios [17] indicating the soundness of this simplified approach to this complex problem. The agreement of the scaling results with the exact solution also established the adiabatic flame temperature as the characteristic flame temperature T_f .

2.1.3 Solution For the Radiative

Regime: The way radiation couples into flame spread is quite complex.

Radiation losses from the surface and gas to the environment drain heat from the otherwise adiabatic flame depressing the flame temperature and, therefore, indirectly affecting the spread rate. Radiation from the flame to the environment and surface re-radiation act as a loss mechanism, reducing the net heat flux to the solid and, hence, resulting in a drop in the spread rate. To sustain the radiative losses, the conduction heat transfer to the surface is

enhanced [18] as the flame moves closer to the surface. Finally, part of the gas radiation tends to

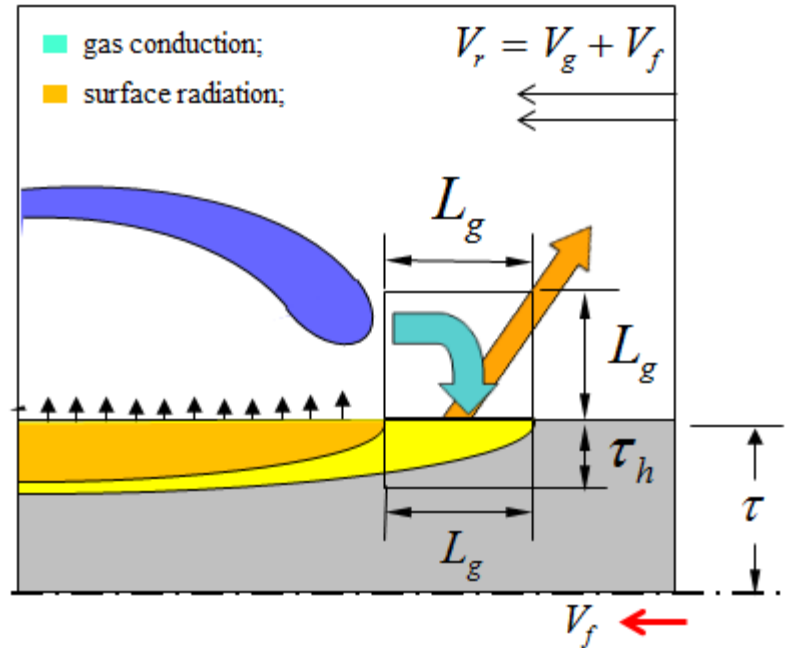


Fig. 3 Only surface radiation is included as a representative radiative effects in the energy balance

compensate the surface radiative losses. By including only surface radiation in the analysis (see Fig. 3) the essential features of radiative effects can be captured as long as gas radiation acts as a net loss mechanism. Indeed there is computational evidence [19,20] suggesting that the radiation feedback is overpowered by radiative losses from the flame to the environment as long as the atmosphere in which the flame spread is not vitiated [21] with radiating species such as carbon dioxide.

With surface radiation representing all the radiative losses (using an effective ε gas radiation can be indirectly accounted for), the energy balance of Eq. (4) is expanded as follows.

$$V_f \rho_s c_s \tau_h W (T_v - T_\infty) + \varepsilon \sigma (T_v^4 - T_\infty^4) L_{gx} W \sim \lambda_g (T_f - T_v) W \quad (7)$$

The equation can be non-dimensionalized as follows.

$$\left(\eta_f^2 + \eta_f \eta_g \right) \frac{\tau_h}{\tau} - (\eta_f + \eta_g) + \mathfrak{R}_0 \sim 0$$

$$\text{where, } \mathfrak{R}_0 \equiv \frac{1}{F^2} \frac{\rho_s c_s}{\rho_g c_g} \frac{\varepsilon \sigma \tau}{\lambda_g} \left(\frac{T_v^4 - T_\infty^4}{T_v - T_\infty} \right), \quad \eta_g \equiv \frac{V_g}{V_{f, \text{thermal, thin}}} \quad \text{and} \quad \eta_f \equiv \frac{V_f}{V_{f, \text{thermal, thin}}} \quad (8)$$

Note that \mathfrak{R}_0 arising out of above non-dimensionalization is identical to the radiation parameter \mathfrak{R}_s we derived from time-scale consideration. As expected, the thermal thin limit $\eta_{f, \text{th, thin}} \sim 1$ is recovered when $\mathfrak{R}_0 = 0$ and $\tau_h = \tau$. To obtain a more general solution, τ_h / τ for a thick fuel can be expressed using Eq. (3)

$$\frac{\tau_h}{\tau} \sim \min \left(1, \frac{\Omega}{F} \frac{1}{\sqrt{\eta_f (\eta_f + \eta_g)}} \right) \quad \text{where, } \Omega \equiv \sqrt{\frac{\lambda_s \rho_s c_s}{\lambda_g \rho_g c_g}}. \quad (9)$$

The energy balance equation, Eq. (8), is solved in both the thick and thin limit producing

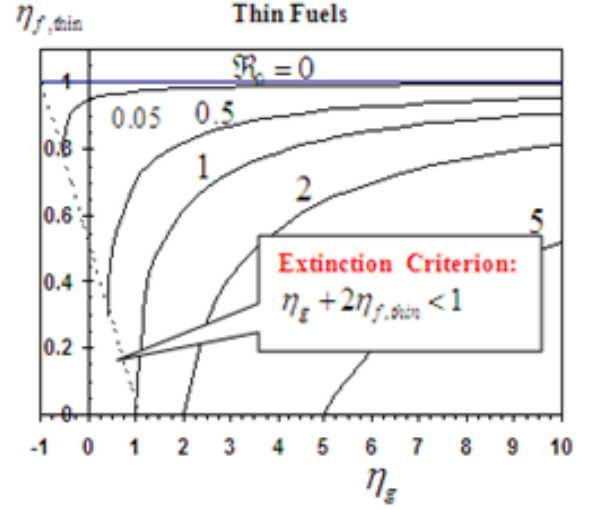


Fig. 4 Thin fuel spread rate as a function of opposed-flow velocity with the radiation number as a parameter as predicted by Eq. (10)

$$\text{Thin Limit: } \eta_{f, \text{thin}} \sim \frac{1 - \eta_g}{2} + \frac{1}{2} \sqrt{(1 + \eta_g)^2 - 4\mathfrak{R}_0} \quad (10)$$

$$\text{Thick Limit: } \eta_{f, \text{thick}} \sim \frac{F^2}{\Omega^2} \eta_g \left(1 - \frac{\mathfrak{R}_0}{\eta_g} \right)^2 \quad (11)$$

Obviously, for $\mathfrak{R}_0 = 0$ and/or $\eta_g \rightarrow \infty$, the thermal limits are recovered. The effect of opposing flow velocity and radiation are decoupled through the parameters η_g and \mathfrak{R}_0 in these expressions for spread rate, which are plotted in Fig. 4 for thin fuels for several values of the radiation parameter \mathfrak{R}_0 .

Opposed-flow flame spread extends down to $\eta_g = -\eta_f$. Notice the two types of extinction predicted by Eq. (10) based on the value of \mathfrak{R}_0 : (i) $\eta_g < \mathfrak{R}_0$ for $\mathfrak{R}_0 > 1$, and (ii) $\eta_g < 1 - 2\eta_{f, \text{thin}}$ for $\mathfrak{R}_0 < 1$ leads to a complex number as a solution, which we interpret as flame extinguishment. For a quiescent environment $\eta_g = 0$ and the extinction criterion reduces to $\mathfrak{R}_0 > 0.25$. The parabolic flight data [22] for flame spread over thin PMMA qualitatively support this predicted trend for thin fuels.

For thick fuels, Eq. (11) when plotted in Fig. 5, clearly shows zero spread rate when the radiation number exceeds the non-dimensional opposed-flow velocity, that is, $\mathfrak{R}_0 > \eta_g$. The DARTFIRE experiments [23] for flame spread over thick PMMA lends qualitative supports to the trends shown in **Error! Reference source not found.**. However, experimental validation of extinction criterion indicated by this analysis still awaits further experimental data that can only be gathered in high duration experiments offered by the International Space Station.

2.1.4 Extinction Criteria: The spread rate expressions of Eq. (11) can be used to establish criterion for flame extinguishment. As can be seen from **Error! Reference source not found.**, there are two types of extinction behavior. For $\mathfrak{R}_0 \geq 1$, steady flame cannot be sustained for both thin and thick fuels if $\eta_g < \mathfrak{R}_0$, a criterion that is independent of fuel thickness (note that both \mathfrak{R}_0 and η_g are proportional to fuel thickness). For $\mathfrak{R}_0 < 1$, the thick fuel criterion remains unaltered. However for thin fuels, the

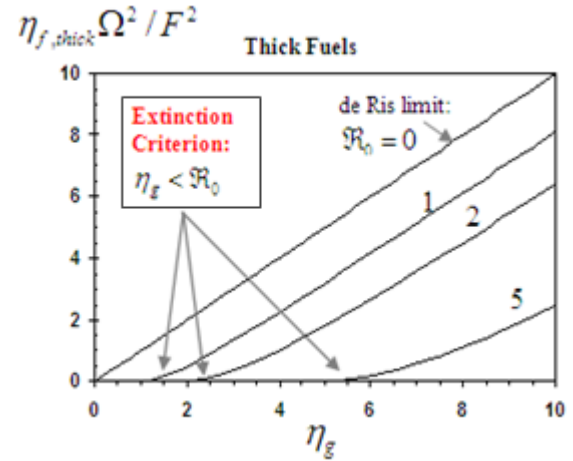


Fig. 5 Thick fuel spread rate as a function of opposed-flow velocity with the radiation number as a parameter as predicted by Eq. (11).

spread rate assumes complex values, an indication of extinguishment, when $\mathfrak{R}_0 \geq (1 + \eta_g)^2 / 4$. From these criteria it is possible to determine an expression for critical opposed-flow velocity below which steady spread cannot be sustained.

In a completely quiescent environment $\eta_g = 0$. The spread rate in a quiescent zero-gravity environment can be simplified from Eq. (10) as

$$\text{Quiescent Limit: } \eta_0 \sim \frac{1}{2} + \frac{1}{2} \sqrt{1 - 4\mathfrak{R}_0} \quad (12)$$

Only for $\mathfrak{R}_0 > 0.25$, spread rate value the above equation can be real, signaling a flame extinction criterion in a quiescent environment for any fuel. This can be converted into dimensional form in terms a critical fuel thickness above which $\mathfrak{R}_0 > 0.25$. That is,

$$\text{Quiescent Extinction Criterion: } \tau > \tau_{cr,0} \quad \text{where, } \tau_{cr,0} = \frac{\rho_g c_g \lambda_g}{\rho_s c_s \varepsilon \sigma} \left(\frac{T_v - T_\infty}{T_v^4 - T_\infty^4} \right) \frac{F^2}{4} \quad (13)$$

Note that an extinction thickness can be found even for 100% oxygen level. Also note that the critical thickness is proportional to ambient density ρ_g and hence can be changed by changing the ambient pressure. Guided by this theory, we select the physical fuel thickness and ambient pressure to control the non-dimensional fuel thickness, $\tau / \tau_{cr,0}$, in the proposed experiments.

2.2 Computational Approach

A numerical model capable of reproducing existing theoretical results and generating reasonable agreement with ground based experiments is employed to investigate the mechanism of flame extinguishment in a microgravity environment. For validating the model, we have conducted downward flame spread tests in a specially developed apparatus called the flame stabilizer [24] and compared the measured temperature fields for spread over thin sheets of PMMA and filter paper with the computational predictions along with the spread rates for different fuels at different thicknesses.

2.2.1 Numerical Model

A schematic of the symmetric half of the flame spread problem in the presence of an opposing flow of strength V_g is depicted in Fig. 6 along with the boundary and interface conditions. In this flame fixed coordinate space, the fuel approaches the flame at the spread rate V_f , one of the desired unknowns, and the oxidizer at $V_f + V_g$. The mathematical model consists of the two-dimensional, steady, elliptic, partial differential equations describing conservation of energy, species mass, total mass, and momentum in the gas phase and ordinary differential equations for the conservation of mass and energy in the solid phase. In the numerical model, the gas and

solid phases are solved sequentially using the SIMPLER algorithm [25] which are coupled by the interface conditions specified. The solution seeks a unique value for the spread rate that anchors the flame leading edge at the desired location, $x = x_{\text{eigen}}$, within the computational domain. This is done by requiring the solid absolute temperature to be a certain value (20% above ambient) at the *eigen* location. The gas-phase balance equations for total mass, fuel, oxygen and nitrogen species mass, x- and y-momentum, and energy can be expressed in the canonical form

$$\frac{\partial}{\partial x}(\rho u \phi) + \frac{\partial}{\partial y}(\rho v \phi) = \frac{\partial}{\partial x} \left(\Gamma_{\phi} \frac{\partial \phi}{\partial x} \right) + \frac{\partial}{\partial y} \left(\Gamma_{\phi} \frac{\partial \phi}{\partial y} \right) + \dot{S}_{\phi}''' \quad (13)$$

where the meaning of each variable is defined in Table 1.

For thin fuels, with temperature T_s remaining constant across the fuel thickness, a one-dimensional energy equation in terms of a variable fuel density can be written as

$$-\tau \rho_s c_s V_f \frac{dT_s}{dx} + \dot{m}_F'' \left[\Delta h_v^o + (c_g - c_s)(T_s - T_{\infty}) \right] = \lambda_g \left. \frac{\partial T}{\partial y} \right|_{y=0+} - \varepsilon_s \sigma T^4 \quad (13)$$

$$\dot{m}_F'' = A_s \rho_s \tau e^{-\frac{E_s}{RT_s}} = \frac{d(\rho_s \tau V_f)}{dx} \quad (13)$$

The mass equation allows the fuel to burnout downstream when the fuel density reaches a preset

Eqn.	ϕ	Γ_{ϕ}	\dot{S}_{ϕ}'''
Mass	1	0	0
x-mom	u	μ	$-\partial p / \partial x$
y-mom	v	μ	$-\partial p / \partial y$
Fuel	y_F	μ / c_g	$-B_g \rho^2 y_O y_F \exp(-E_g / RT)$
O ₂	y_O	μ / c_g	$-s B_g \rho^2 y_O y_F \exp(-E_g / RT)$
N ₂	y_N	μ / c_g	0
Energy	T	μ / c_g	$(\dot{m}_F''' \Delta h_{cE}^o + \dot{q}_R''') / c_g$

Table 1. Meaning of the generic variables in the canonical equation.

burnout value.

The properties used for PMMA and ashless filter paper are listed in Table 3. The radiation source term is obtained by using a thin gas emission approximation with a constant Planck mean absorption coefficient a_p using a global balance method [26] in which an effective a_p is calculated by equating gas emission calculated by the thin-gas emission approximation with a more accurate comprehensive solution. In the comprehensive model a computational box is placed around the

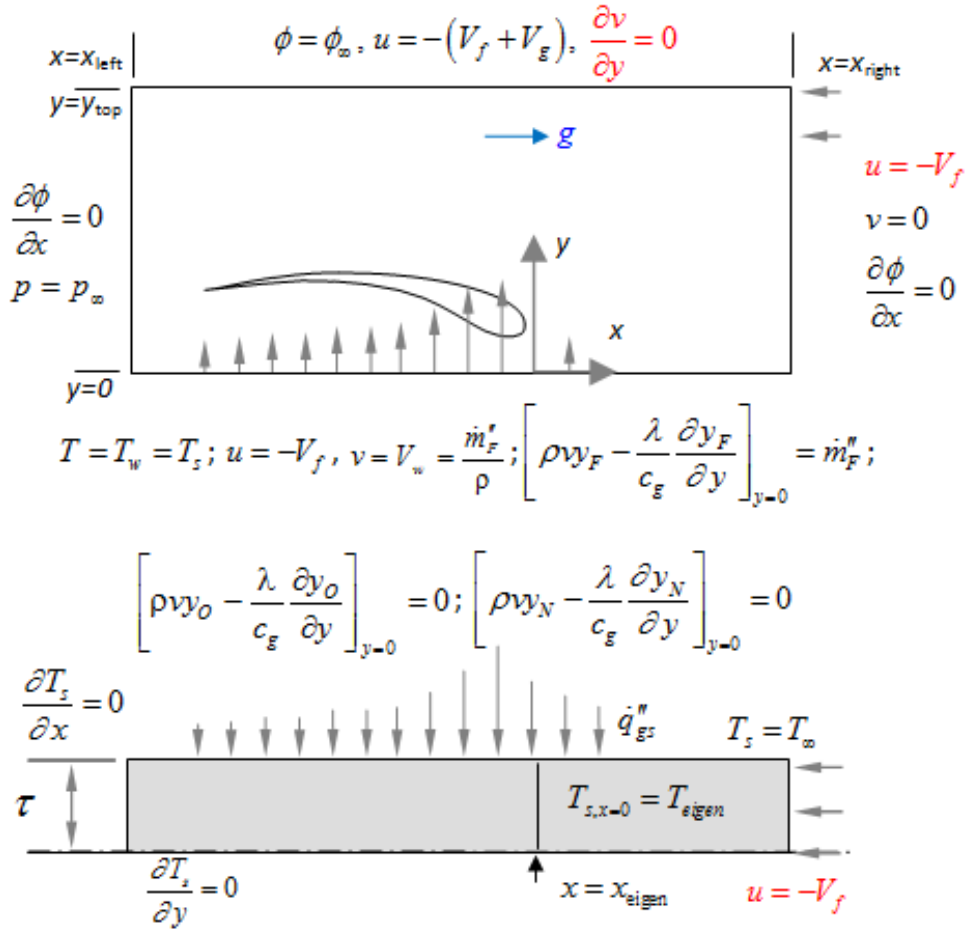


Fig. 6 Interface and boundary conditions used in solving the governing equations.

calculated species and temperature field in the gas phase. The distribution of radiative flux is then calculated at each surface of the box, taking into account the finite width (equal to the fuel width) of the box. At each point on a surface, 400 lines of sight covering the entire hemisphere exposed to the flame are integrated to obtain the heat flux. Finally, heat flux over all the six surfaces are integrated to yield the radiative loss from this computational box. The value of a_p calculated by such global balance is found to vary from 1.5 to 3 m^{-1} .

The computation is started with an initial guess of the spread rate V_f and gas phase conserved properties. After a few iterations, heat flux \dot{q}_{gs}'' from the gas to the solid surface is calculated. The solid phase energy and mass equations are then solved to determine a V_f that produces a specified temperature $T_{\text{eigen}} = 1.2T_\infty$ at a specific location x_{eigen} (25 mm downstream of the upstream boundary). The temperature, mass flux distribution, and the spread rate obtained from the solid phase solution are used as the boundary conditions for the gas phase equations, which are

Phase	Symbol	PMMA	Cellulose	Unit
Solid	ρ_s	1190	518.7	kg/m ³
	c_s	1.465	1.256	kJ/(kg.K)
	Δh_v°	0.941	0.368	MJ/kg
	Δh_c°	-25.9	-16.74	MJ/kg
	$\Delta h_{CE,21\%}^\circ$	-24.45	-15.624	MJ/kg
	$\Delta h_{CE,50\%}^\circ$	-17.05	-11.671	MJ/kg
	E_s	81.867	249.42	MJ/kmol
	A_s	8.78×10^5	7.8×10^{16}	1/s
	ε_s	1	1	
Gas	c_g	1.183	1.183	kJ/(kg.K)
	$\lambda_{g,700K}$	0.052	0.052	W/(m.K)
	$\mu_{g,700K}$	40.3	40.3	kg/(m.s)
	B_g	8.928×10^7	6.17×10^7	m ³ /(kg.s)
	E_g	83.72	62.99	MJ/kmol
	s	1.92	1.185	

Table 2. Fuel and gas property values [43] used in computations.

solved to produce a better heat flux distribution. Iterations between the two phases are continued until convergence is achieved in all results. The choice of the *eigen* condition and the *eigen temperature* has no role other than pinning the flame leading edge at a location of choice.

2.2.2 Equilibrium Combustion Model

The numerical model employs a global single-step Arrhenius kinetics to model gas phase combustion. The computed flame size, as captured by the reaction zone, and the computed flame temperature consistently showed higher values when compared to downward spreading

experiments. As an alternative to multi-step kinetics, we introduced an equilibrium based correction to the enthalpy of combustion. A rich internet application (RIA) has been developed [27] at our laboratory and made accessible to the public for computing equilibrium composition and flame temperature.

As shown in Fig. 7, calculating equilibrium composition has never been easier. Once the RIA is launched (from test.sdsu.edu, select the RIAs tab, and click on Reaction Chamber Simulator icon), select the Known Heat Transfer tab where the default heat transfer is zero (for adiabatic combustion). Select PMMA from the fuel selector, set the oxygen level with the aid of the slide bar, select the equilibrium species, and click Calculate. The temperature is calculated as 2850 K as opposed to 4118 K for complete combustion. For both PMMA and cellulose combustion, it can be shown (through selective elimination) that a set of ten species in the

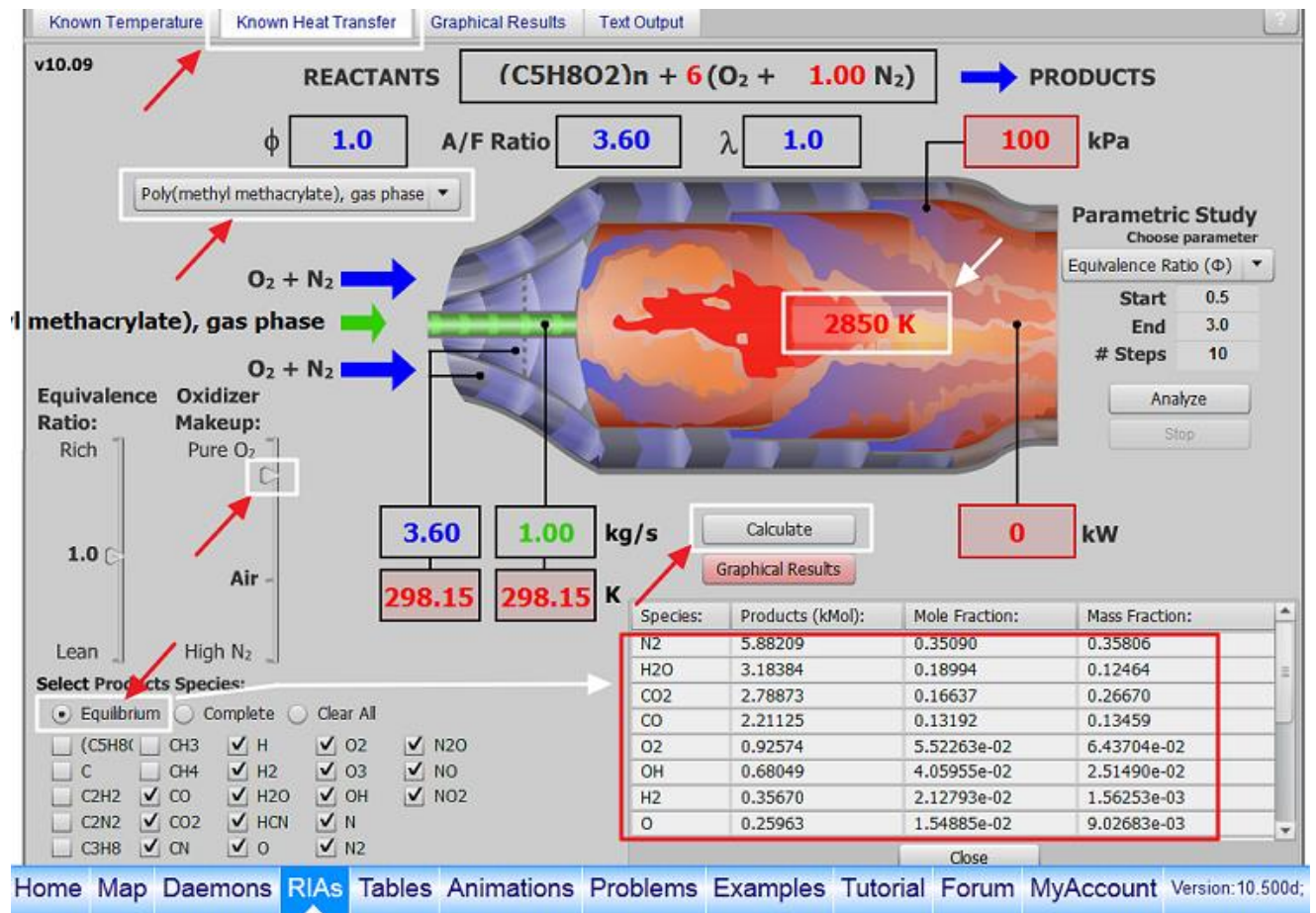


Fig. 7 Equilibrium composition and adiabatic equilibrium flame temperature for PMMA burning in 50-50 mixture of O₂/N₂ as calculated by the RIA. The RIA is available to the community from <http://test.sdsu.edu>.

products - CO₂, H₂O, CO, O₂, NO, OH, H₂, O, H, N₂ - are sufficient to capture energetics of

equilibrium combustion, producing the same equilibrium temperature as a full set of possible products would. This finding is valid for different oxygen levels and pressures as well. Of course the equilibrium composition is a function of fuel and oxidizer composition and pressure.

Using the equilibrium composition produced by the RIA (see Fig. 7), the enthalpy of combustion is recalculated at different oxygen levels and show in Table 3. Use of this approach will be shown to produce much better agreement with detail experimental measurements of the field variables.

2.3 Experimental Approach

The proposed space based experiments will produce valuable data on field variables such as temperature and species concentrations which will help us test our hypothesis that the asymmetry between the thermal and species fields triggers the unsteady behavior eventually leading to flame extinguishment. To validate the numerical model that will be used to interpret and mine the data from space experiment, we have built two experimental set ups at SDSU, the flame stabilizer [24] and the flame tower [28].

2.3.1 The Flame Stabilizer

A spreading flame poses a considerable challenge for obtaining detailed information on its structure. Measurement of the temperature and velocity field, for example, could be of great value for evaluating modeling results. Hirano et al. [29] measured the velocity field by particle tracing methods and used fine wire thermocouples to obtain temperature data for flame spread over thin cellulosic fuels. Fernandez-Pello [30] used thermocouple probes, interferometry, radiometer measurements, gas-phase chromatography, and particle-tracking photography to conclude that the dominant mode of heat transfer in flame spread over thermally thick PMMA is conduction through the solid phase. Fernandez-Pello et al. [31] also performed downward flame spread experiments on thick PMMA rods to measure temperature and velocity fields, reaching the same conclusion that conduction through the solid phase is the dominant mechanism of flame spread. However, Ito et al. [32] used holographic interferometry to conclude just the opposite, that is, that gas phase conduction is more dominant for forward heat transfer, a conclusion that has been supported by later numerical models [33].

The purpose of the flame stabilizer is to perform a coordinate transformation in real time for a downward spreading flame. A flame spreading in an opposed-flow environment is an unsteady phenomenon from a laboratory reference even if the spread rate is steady. Steady-state analytical models of the spread are based on flame fixed coordinates in which the fuel approaches the flame at a relative velocity V_f , the spread rate, and the oxidizer approaches the flame at a relative velocity $V_g + V_f$, where V_g is the opposing flow velocity. For downward

flame spread in a quiescent environment, $V_g = 0$ at a sufficiently large distance upstream of the flame leading edge. The flame stabilizer mimics this modeling approach by moving the fuel upward at V_f , thereby making the flame stationary. However, the boundary conditions are slightly altered because the oxidizer still moves towards the flame at V_g and not $V_g + V_f$. The hypothesis to be tested is that this slight alteration in the flow boundary condition has negligible effect on the flame spread rate and flame structure because V_f is small compared to the characteristic buoyancy induced opposing flow velocity.

2.3.1.1 Stabilizer Hardware A schematic of the experimental hardware is shown in Fig. 8. The apparatus relies on vertical velocity control of the fuel sample. A linear motion assembly was chosen [19] consisting of a motor, indexer, lead screw and nut, carriage, and a pair of guide rail

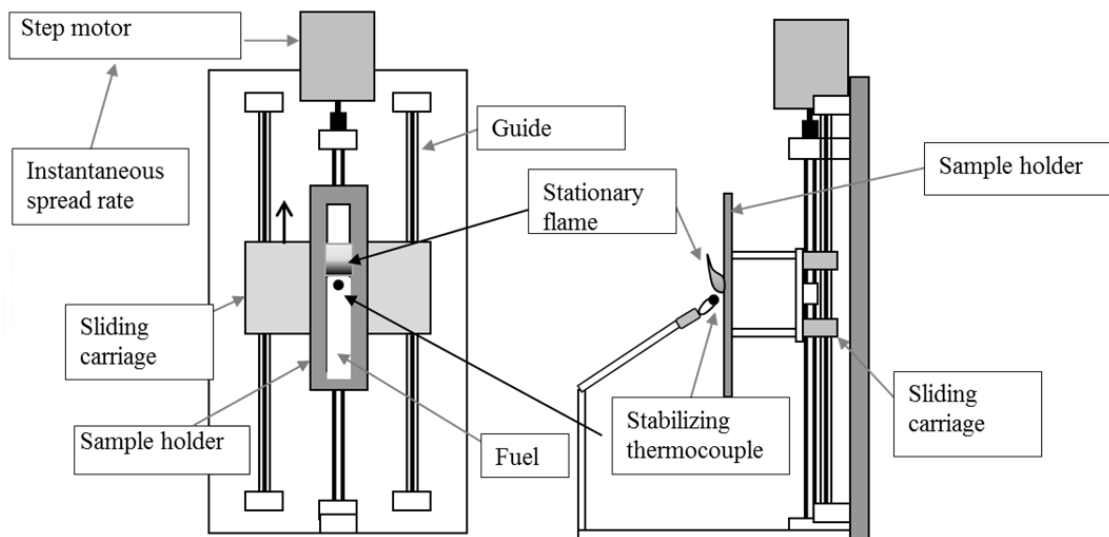


Fig. 8 The stabilizing thermocouple is attached to the test stand while the sample is mounted on a carriage moved by the PID control algorithm in the opposite direction of the spread to maintain a constant thermocouple signal, thereby arresting the flame motion and anchoring the leading edge just above the thermocouple.

and pillow blocks. The motor selected is a Compumotor AX83-135 two-phase permanent magnet hybrid step motor. The Compumotor is controlled by an indexer that processes commands sent from a serial port of the controlling computer and produces an analog voltage signal for moving the motor. This motion controller produces an angular velocity range of 0.01 rev/sec to 50.00 rev/sec with a resolution of 12800 steps per revolution. A steel lead screw was chosen with a pitch of 2 mm and a diameter of 10 mm, creating a linear velocity range of 0.02 mm/s to 100 mm/s for the motion system. An Acetal-Teflon and Silicone anti-backlash nut was selected to transfer the load from the screw to the carriage. This nut was designed for a

maximum preload of 5.2 kg and a maximum torque of 0.28 Nm. The Precision Industrial Components Corporation manufactured both the lead screw and the nut. Thompson Industries manufactured the guide rails and pillow blocks. Two kill switches, connected to the AX indexer, were used at the top and bottom of the ball screw to prevent the nut from accidentally hitting the end support bearings.

The sample holder was made of two thin aluminum (or steel) plates 45 cm long hinged at one end with a rectangular slot of width 3 cm (equal to the sample width) cut through both plates. A thin fuel sample (ashless filter paper or thin PMMA film) is placed between the two plates, which are pressed against each other using magnets (for the steel sample holder) or clips (for the aluminum). The sample holder is then secured on the carriage with wing nuts. The length of the fuel sample, which controls the duration of the experiment, L/V_f , is limited by the length of the lead screw. In our current set up, a burn time of more than 150 s is typical for flame spread over 0.16 mm thick filter paper. Ignition is performed with a butane lighter or a heating wire. An EICO 1078 AC variable current power supply was used to produce 2.5 amps at 10 V across a 0.009" diameter nichrome wire touching the top front surface of the fuel. We found this method of ignition to have no effect on the spreading behavior of a flame.

We selected a 0.01" diameter K type thermocouple, attached to the test stand (fixed relative to the laboratory coordinates), as the sensor to locate the leading edge of a flame. A K type thermocouple has a temperature range of 0 to 1370 °C. Selection of such a small diameter thermocouple reduces any heat-sink effect on the flame front and provides a fast response time, a necessity for the stability of the control system. A National Instruments USB-9211A device with built-in sensors for cold-junction compensation is used for reading the thermocouple signal with a 24 bit resolution.

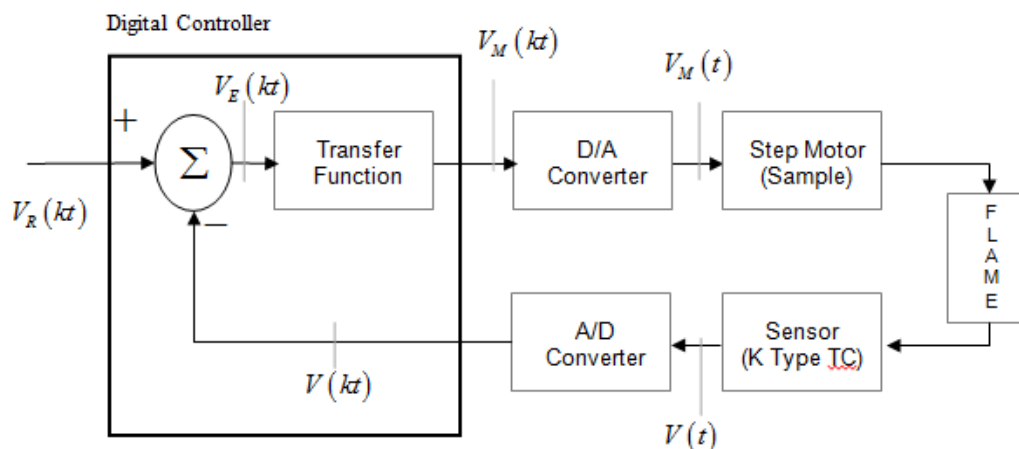


Fig. 9 The proportional, integral, differential (PID) control algorithm tries to keep the thermocouple signal a constant by adjusting the signal to the motor..

2.3.1.2 PID Control Algorithm A closed loop feedback control algorithm was implemented using LabVIEW to stabilize a spreading flame. A block diagram for the digital control system is shown in Fig. 9. In this control loop, $V(t)$ is the voltage signal from the thermocouple that is fixed in the laboratory coordinates. As the flame approaches the thermocouple, $V(t)$ increases. The digital reading of this voltage is represented by $V(kt)$, where k is an integer value representing the number of passes through the control loop. The goal of the control algorithm is to keep $V(kt)$ as close as possible to the reference voltage V_{ref} ; that is, to minimize the error function $V_{\varepsilon}(kt) \equiv V_{\text{ref}} - V(kt)$. After trying several different control algorithms, we decided that PID (proportional gain, integral time, and derivative time) control was the best choice. In this algorithm, the output signal $V_M(kt)$ is determined using proportional, integral, and derivative information determined from the error signal. The discretized *velocity algorithm* for a PID controller is:

$$V_M(k) = V_M(k-1) + K \left[\{V_{\varepsilon}(k) - V_{\varepsilon}(k-1)\} + \frac{\Delta t}{t_i} V_{\varepsilon}(k) + \frac{t_d}{\Delta t} \{V_{\varepsilon}(k) - 2V_{\varepsilon}(k-1) + V_{\varepsilon}(k-2)\} \right] \quad (14)$$

In this equation, K , t_i , and t_d are the proportional gain coefficient, the integral time, and the

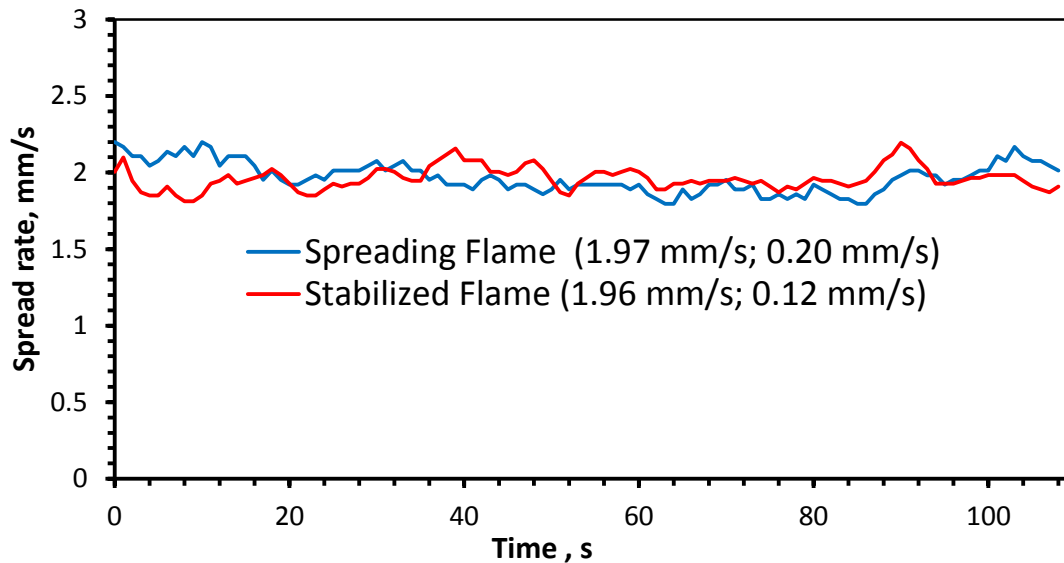


Fig. 10 Comparison of flame spread rates between downward spreading flame and flame rendered stationary by the flame stabilizer.

derivative time, respectively. The proportional gain coefficient affects the responsiveness of the feedback control and introduces a steady-state error. With the addition of integral control, the steady-state error can be eliminated at the expense of some instability. The derivative time

constant is analogous to a damping coefficient that can be increased to mitigate the instability introduced by the integral control. Optimization of the flame stabilizer reduces to finding an optimal set of values for K , t_i , and t_d . These coefficients were found experimentally by first using only proportional control, and then successively introducing integral and differential controls. For our particular set up, the values found were 7.05, 0.2 s and 1.5 s respectively.

2.3.1.3 Flame Spread Rate To determine how spread rates obtained from the stabilizer compare with downward spread rates, two successive experiments were performed, one with the stabilizer turned off and one with the stabilizer turned on. Spread rates obtained from the stabilizer and from the video analysis of the downward spreading flame are compared in Fig. 10. The average spread rates are 1.972 mm/s from the stabilizer and 1.973 mm/s from the Spotlight analysis of the downward spreading flame. The results clearly establish that the flame stabilizer produces a spread rate that is within the experimental uncertainty of video analysis of spread rate of a

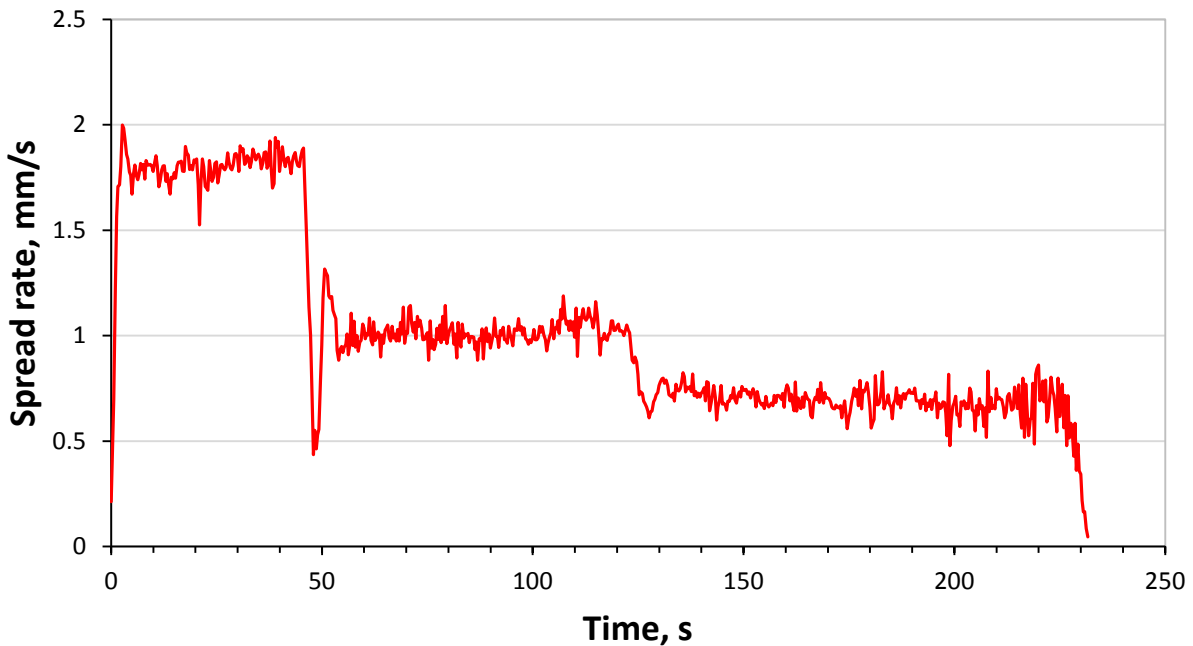


Fig. 11 The flame stabilizer responds to fuel of increasing thicknesses.

downward spreading flame. It should be stressed that, while the video analysis tracks a spot on the pyrolysis front, the thermocouple stabilizer sensor is located in the gas phase. The variability in spread rate (as measured by the standard deviation) produced by the stabilizer was found to be about the same, around 0.1 mm/s, when the experiments were repeated with different thermocouple locations across the width and at different distances away from the fuel surface.

The response time of the apparatus was tested by stacking two and three sheets of filter papers and letting the stabilizer adjust to the changing fuel thicknesses in a single experiment. As shown in Fig. 11, the stabilizer responds almost in real time to the changing spread rate.

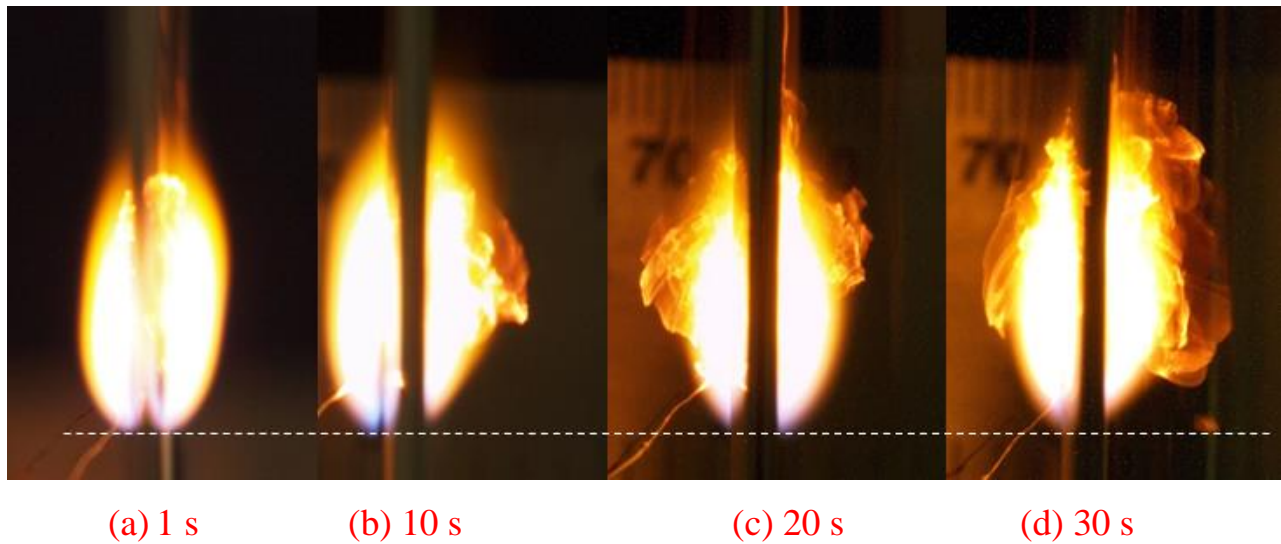


Fig. 12 Side view of the stabilized flame with four different camera exposure time.

2.3.1.4 The Stabilized Flame The flame stabilizer converts a moving flame into a stationary one. The flame shape remains frozen in time allowing time for field measurement. As shown in Fig. 12, the flame shape remains relatively unchanged over time.

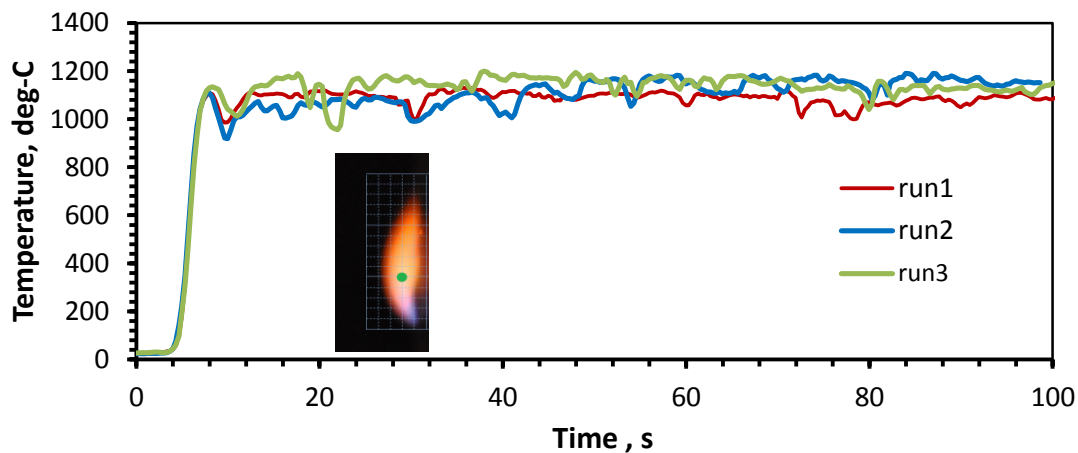


Fig. 13 Measuring the average temperature field of the stabilized flame.

2.3.1.5 Field Measurement With the flame rendered stationary for about 150 s by the Flame stabilizer, a 75 μm diameter K type thermocouple connected to a x-y linear motion system is used to collect temperature vs. time data at different x-y locations. The repeatability of the data (shown in Fig. 13) indicates a steady field; however, outside the flame and in the far downstream regions, considerable fluctuation is found in the measurements.

For a spreading flame, fluctuations in the reading comes from both spatial and temporal variations. As a result when the temperature contours are reconstructed by converting the temperature vs time signal to temperature vs. position (using the spread rate), only a snapshot of the thermal image is obtained. On the other hand, averaging the temperature signal over time at a given location produces an average flame picture. The contrast between the two cases is shown in Fig. 14. If the measurements of Fig. 14 are repeated, the image corresponding to the spreading flame will change considerably while that for the stabilize flame would alter very slightly change, that too, mostly in the downstream region. It should be noted that the thermocouple could not be positioned closer than 1 mm from the fuel surface.

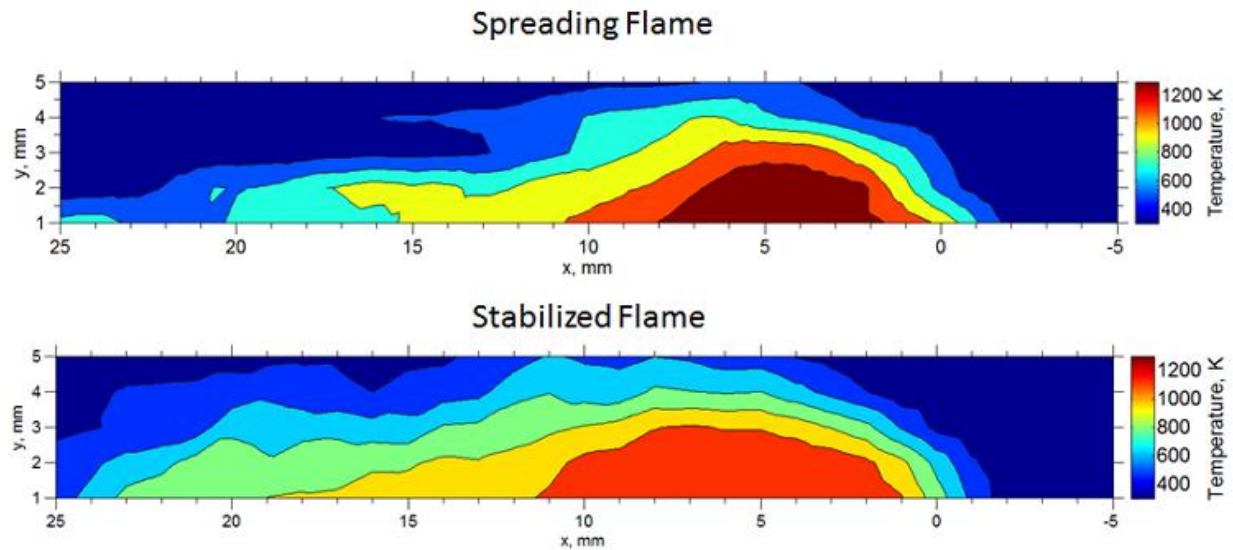


Fig. 14 Temperature field measured by a K type thermocouple for a spreading flame vs. a stabilized flame over 180 μm thin ashless filter paper.

A non-dispersive infrared (NDIR) CO₂ probe is used to measure CO₂ concentration in several locations of the stabilized flame. However, given the temperature sensitivity of the probe, combustion products has to be pumped in through a ceramic tube. The pumping rate, with a maximum of 0.4 L/min, is a concern if it affects the flame. At least for downward spread, we find that the spread rate is minimally affected by it. For a given location of the suction tube

(inside the flame), three different settings of the flow control valve was used to vary the pumping rate and the spread rate produced by the stabilizer (see Fig. 13) does not seem to indicate any significant effect of pumping on the flame. The slight variations seen in Fig. 15 is well within the variability of conducting separate experiments (spread rate is slightly affected by the humidity and room temperature). Of course, in the diffusive environment under the microgravity condition, this conclusion may not be valid and tests in the drop tower will be sought to evaluate the impact, if any, of the suction necessary for measuring CO₂.

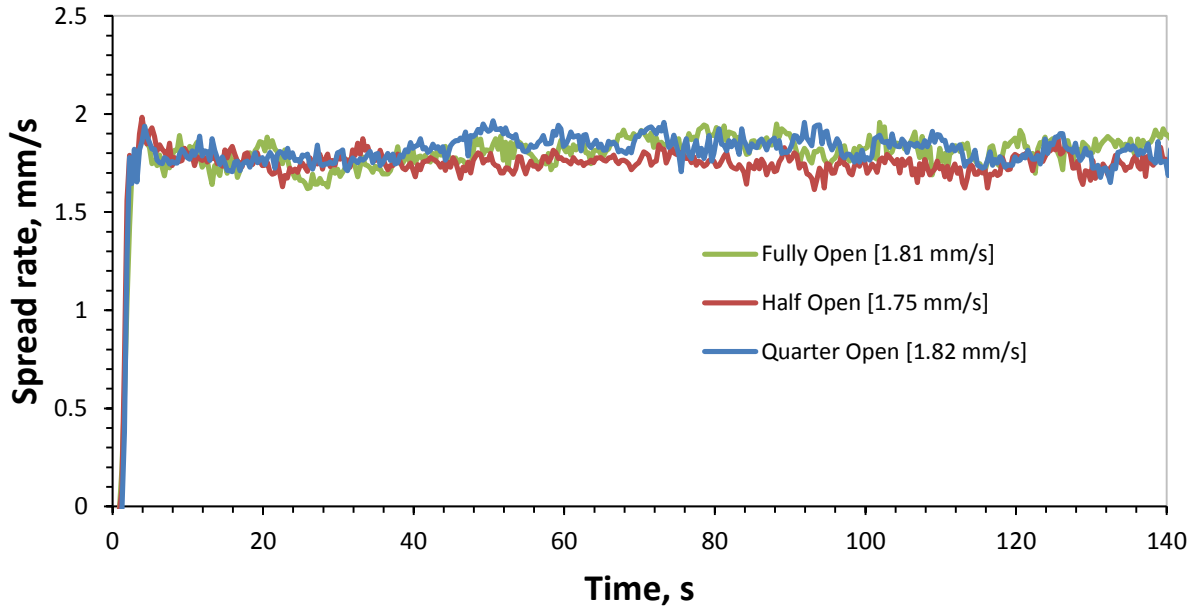


Fig. 15 Pumping by the CO₂ probe with different settings of the valve does not seem to have much effect on the flame spread rate.

Results of CO₂ measurements are consistent with the gas temperature field. At a given location, $x = 10$ mm and $y = 1$ mm, the thermocouple trace is compared with the CO₂ signal in Fig. 14. The CO₂ concentration and the temperature are non-dimensionalized with their equilibrium limits: $\frac{T - T_0}{T_{\text{eq}} - T_0}$ and $\frac{y_{\text{CO}_2} - y_{\text{CO}_2,0}}{y_{\text{CO}_2,\text{eq}} - y_{\text{CO}_2,0}}$ respectively. For combustion of cellulose under atmospheric conditions, the equilibrium RIA [34] can be used to evaluate the equilibrium temperature and CO₂ mole fraction as 2216 K and 0.1633. The plot shows that CO₂ concentration is quite similar to the temperature trace. Of course, the response time of the CO₂ probe is larger and there seems to be slight damping of the signal introduced by pumping. But overall, the CO₂ probe seems to be effective in characterizing the extent of the products field.

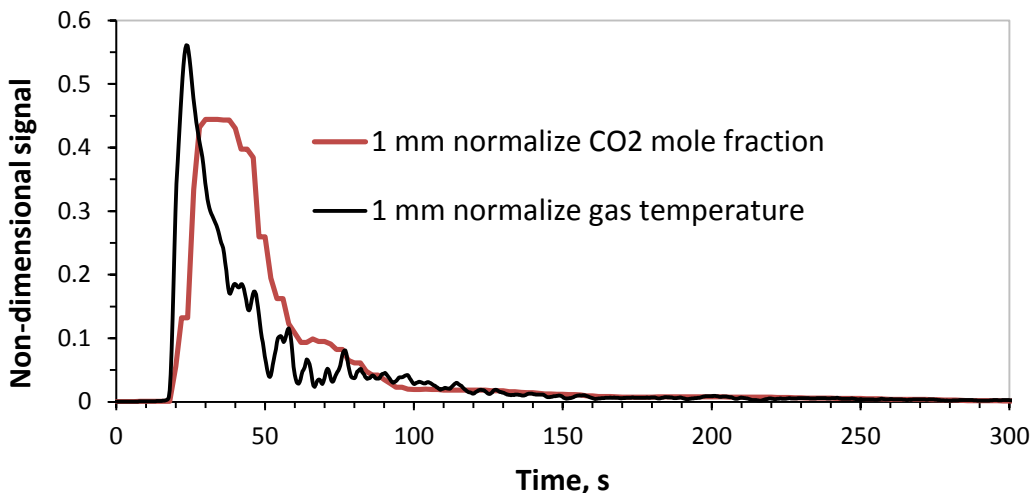


Fig. 16 Measurement of the concentration and temperature at a given location in a spreading flame

The measurements of temperature and CO₂ concentration along the downstream centerline (after the burnout point) in a stabilized flame are compared in Fig 17. Once again we see the similarity between the two signals non-dimensionalized by their equilibrium values (as was plotted in Fig. 16). In the proposed space experiment, we want to examine this similarity and test our hypothesis

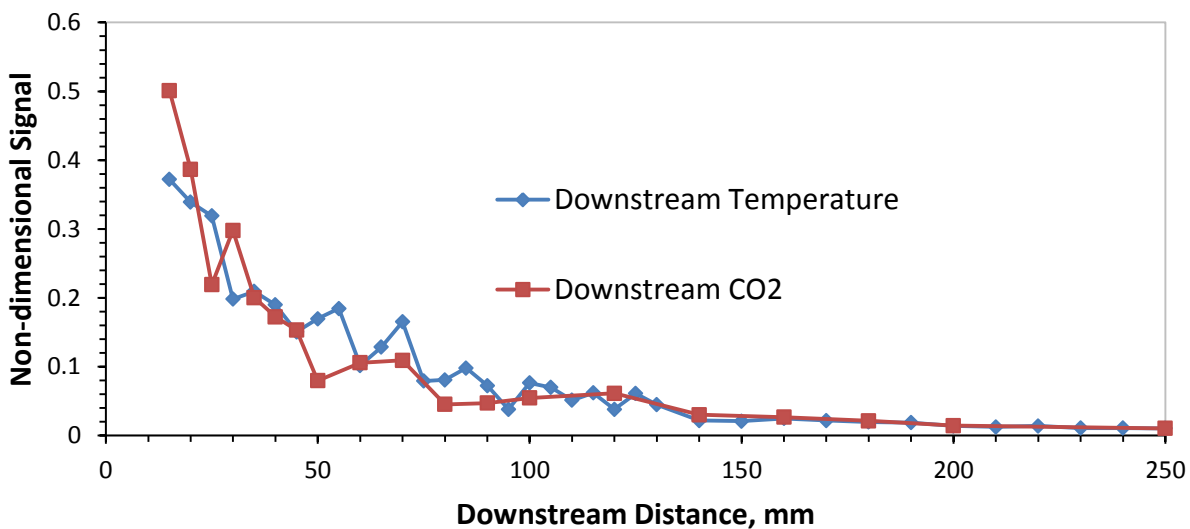


Fig. 17 Non-dimensional temperature and CO₂ concentration along the centerline in a stabilized flame.

that because of radiative losses, the temperature field may shrink in size and shape compared to the products field as represented by CO₂.

2.3.2 The Flame Tower

Most opposed-flow flame experiments have been performed in wind tunnels. However, creating a low velocity field with a known profile is a challenging task. At SDSU we built a 8 m tall vertical steel chamber with a 45 cm x 45 cm square cross-section, which we call the flame tower, inside which a fuel sample mounted on a cart can be traversed up or down with a prescribed velocity. The cart carrying the experimental package is connected by a string going over a pulley at the top of the tower to a counter weight that moves up and down through a vertical tube in opposite direction of the cart. A stepper motor (step angle 0.028125 degree, 12800 steps per shaft revolution, 120 VAC, 5.0 A, max holding torque 5.4 N-m) housed at the top of the tower creates the desired motion by winding or unwinding a separate string connected to the cart. The power supply and the connection to the serial port of the indexer of the motor is run through a electrical

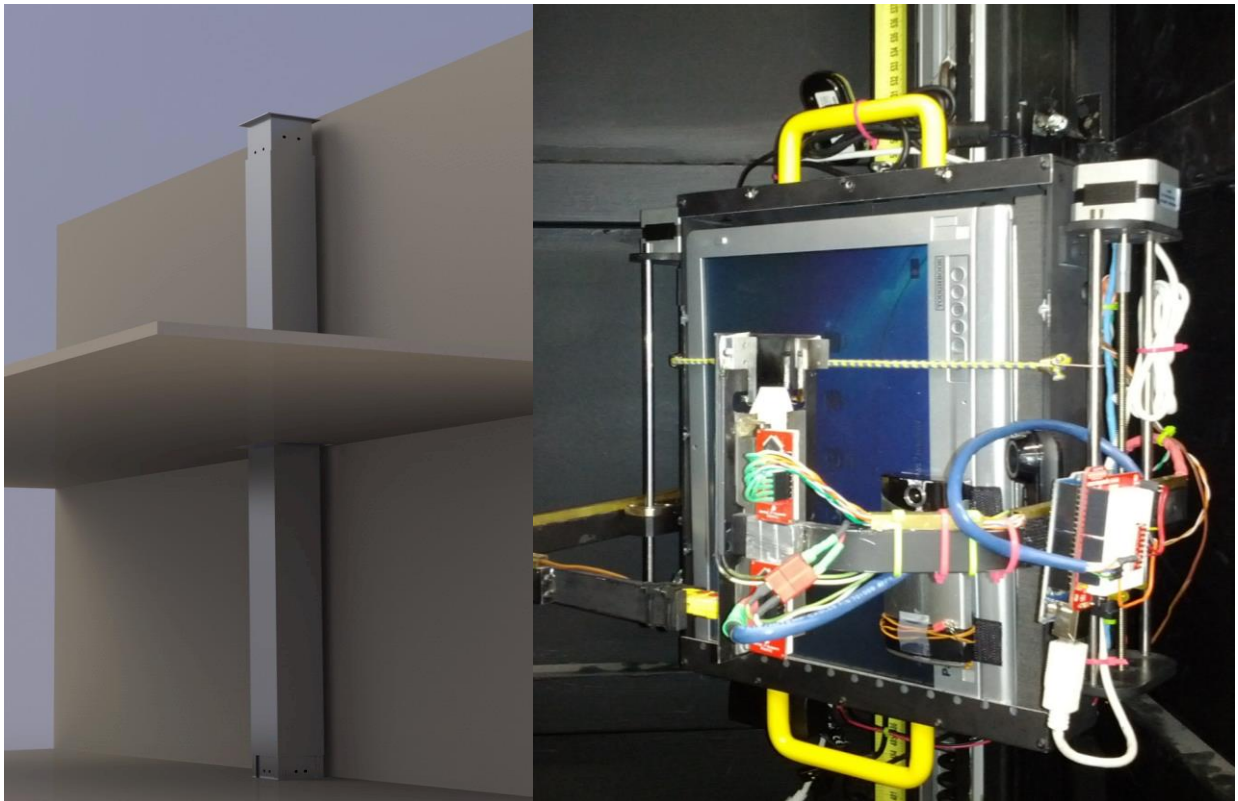


Fig. 18 Eight meter tall flame tower at SDSU inside which a fuel sample can be ignited and traversed up or down at any desired speed upto 2 m/s. The cart carrying the sample is operated by an on-board computer and a micro-controller.

seal.

The velocity of the cart was measured by analyzing a digital high-speed video of a measuring tape attached to the rail from a camera mounted on the cart. The acceleration, velocity

and deceleration profiles matched the command profiles almost exactly. A hot wire anemometer was connected to the cart and placed at several locations to ascertain the flow velocity, which was tested to be reasonably uniform over a 10 cm by 10 cm area upstream of the fuel sample.

The cart, shown in Fig. 18, carries an assembly of fuel sample, igniter, diagnostic system, and an on-board computer all powered by a battery and remotely accessed from outside through wireless network. The fuel sample, 2 cm wide and 10 cm long, is sandwiched between two thin aluminum plates with rectangular cut outs held by an arm attached to the cart. A Kanthal (iron-chromium-aluminum, FeCrAl) alloy igniter wire at the top of the sample holder is connected to the ignition circuit controlled by a micro-controller through the same arm. A second arm is held by a lead screw (1/20.8 TPI) assembly connected to a stepper motor (step angle 1.8°, 200 steps per shaft revolution, 12VDC, 0.33A, maximum holding torque 0.226 kg-force cm). It holds a 125 μm diameter K type thermocouple in front of the flame. During an experiment, the igniter wire is enabled remotely and ignites the top edge of the fuel sample. The moving arm then positions itself at an assumedly constant distance away from the downward propagating flame's leading edge by maintaining a constant set point temperature over the burn duration and a digital video camera captures the side and top view of the spread, allowing independent evaluation of flame spread rate through digital video processing.

2.3.1.5 Data from Flame Tower We have conducted extensive experiments for flame spread over ashless filter paper by varying the flow velocity V_g from positive (opposed-flow) to negative (concurrent-flow) to study the transition of the flame spread from one regime to another under ambient conditions. In each experiment, the cart is moved to one end of the tower and the sample is ignited at the top. The flame spread is monitored through the remote access of the on-board web cam and once the flame reaches a certain distance the cart is moved at the desired velocity.

Position vs. time data from the tracking thermocouple for a particular run at $V_g = 45 \text{ cm/s}$ for a fuel thickness of 180 μm is shown in Fig. 19, which also displays the side view of the flame for the cart in stationary and moving mode. Data that spans the acceleration and deceleration of the cart is discarded, explaining the gap in position vs. time plot. The spread rate decreases from 1.83 mm/s to 1.16 mm/s as the opposing flow velocity increases from 0 (pure downward spread) to 45 cm/s. The flame shape can also be seen to get significantly smaller, indicative of kinetic effect. If the opposing flow is further increased to about 60 cm/s, blow-off extinction is consistently observed.

When the cart is moved upward, we would expect the residence time to increase, thereby, reducing the kinetic effect. On the other hand, if kinetic effect is not significant for pure

downward spread at 21% oxygen level, the radiative effect should reduce the spread rate. Indeed, the data for $V_g = -10$ cm/s, shown in Fig. 20, displays a slight decrease in spread rate, from 1.80 mm/s to 1.76 mm/s. The flame shape shows a slight increase in size. This is exactly what we



Fig. 19 Position vs. time plot and flame shape (side view) for downward flame spread over ashless filter paper (180 μm thin) in ambient conditions with or without an opposing flow.

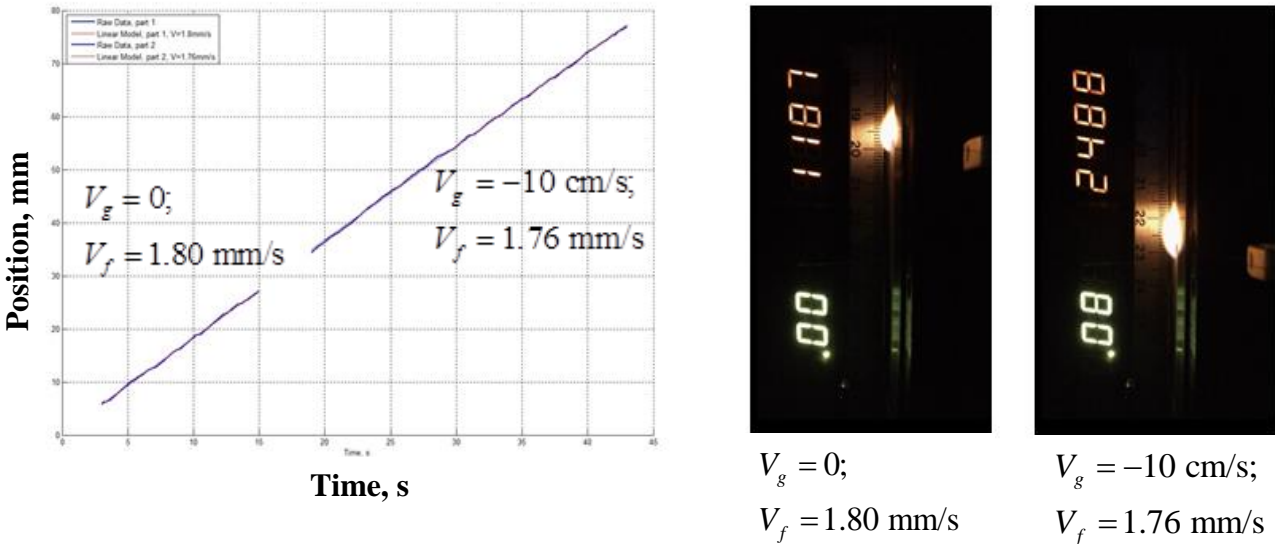


Fig. 20 Position vs. time plot and flame shape (side view) for downward flame spread over ashless filter paper (180 μm thin) in ambient conditions with or without a concurrent flow.

would expect in the microgravity regime as the opposed flow is gradually reduced. In the flame tower, however, any further increase in the upward velocity of the cart begins the process of flipping the flame from the opposed-flow configuration toward concurrent-flow configuration.

The data for $V_g = -35$ cm/s, displayed in Fig. 21, shows an increase in spread rate

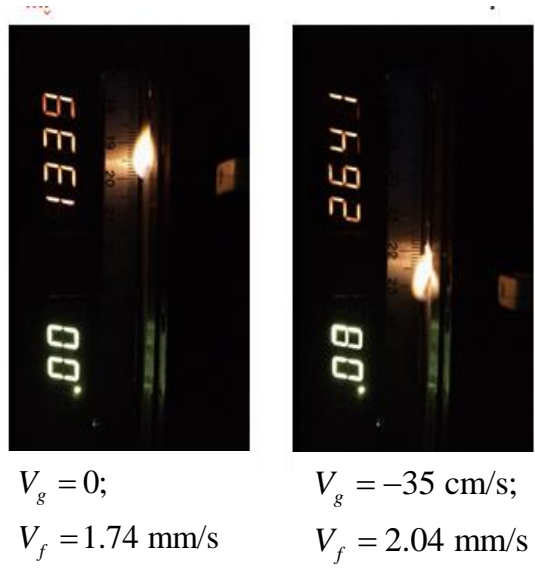
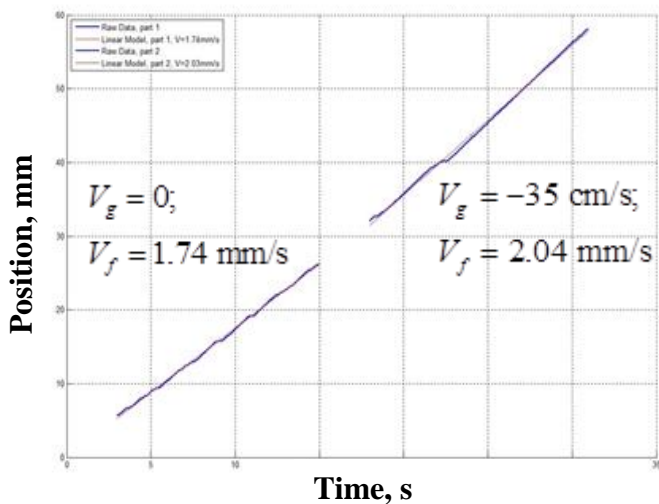


Fig. 21 Position vs. time plot and flame shape (side view) for downward flame spread over ashless filter paper (180 μ m thick) in ambient conditions with or without a concurrent flow.

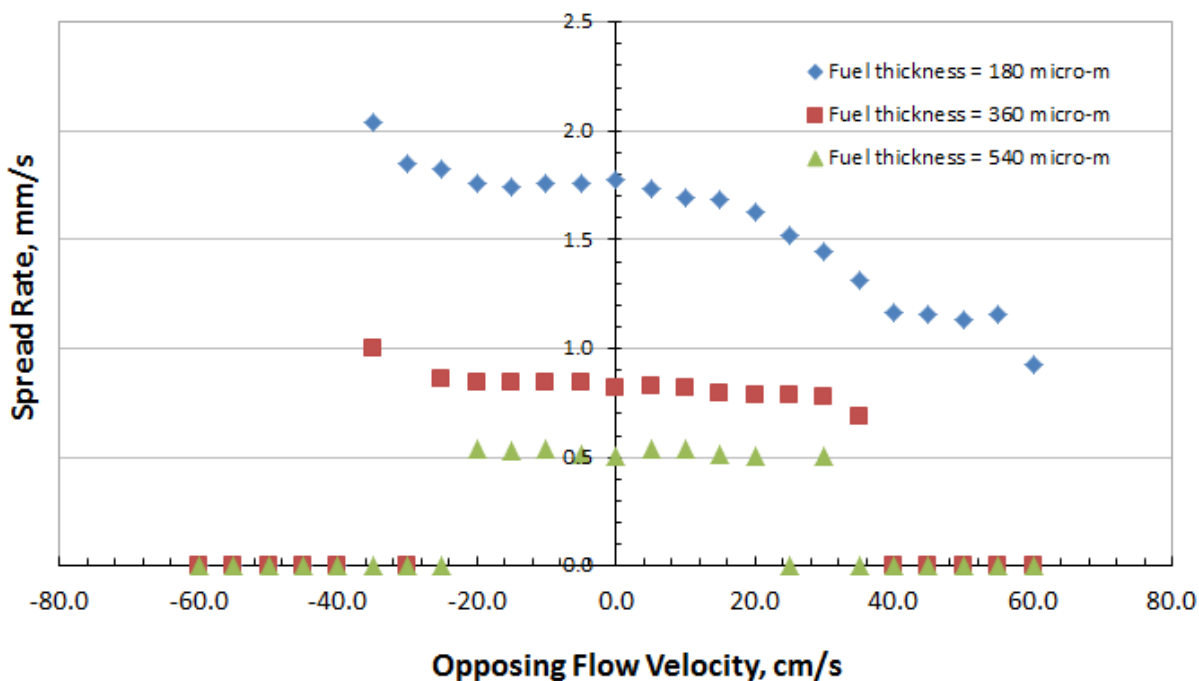


Fig. 22 Data averaged over different runs for flame spread over ashless filter paper of 3 different thicknesses with ambient air as the oxidizer.

from 1.74 mm/s to 2.04 mm/s, which can only be attributed to enhanced heat transfer to the preheat zone of the fuel due to change in flame shape (trying to curve forward) as can be seen in the flame image of Fig. 21.

Spread rate averaged over a number of runs are summarized in Fig. 22. As the opposed flow is increased to about $V_g = 60$ cm/s, blow-off extinction can be seen to occur for a fuel thickness of 180 μm . As the flow velocity is decreased, the spread rate gradually increases as the kinetic effect decreases due to increased residence time. As the residence time is further increased by moving the cart upward (negative V_g), the spread rate shows a slight decreasing trend, perhaps, because of radiative losses kicking in as it occurs in the microgravity regime. For a further increase in upward velocity of the cart, the flame flips around into concurrent flow configuration and the spread rate quickly increases leading to blow-off extinction as the residence time decreases once again. When the fuel thickness is increased by pressing two or three sheets of ashless filter paper together, the results show a drastic decrease in the blow-off extinction velocity, suggesting that blow-off may not be completely controlled by gas phase. We have not found equivalent data in literature or any prevailing theory to explain this result.

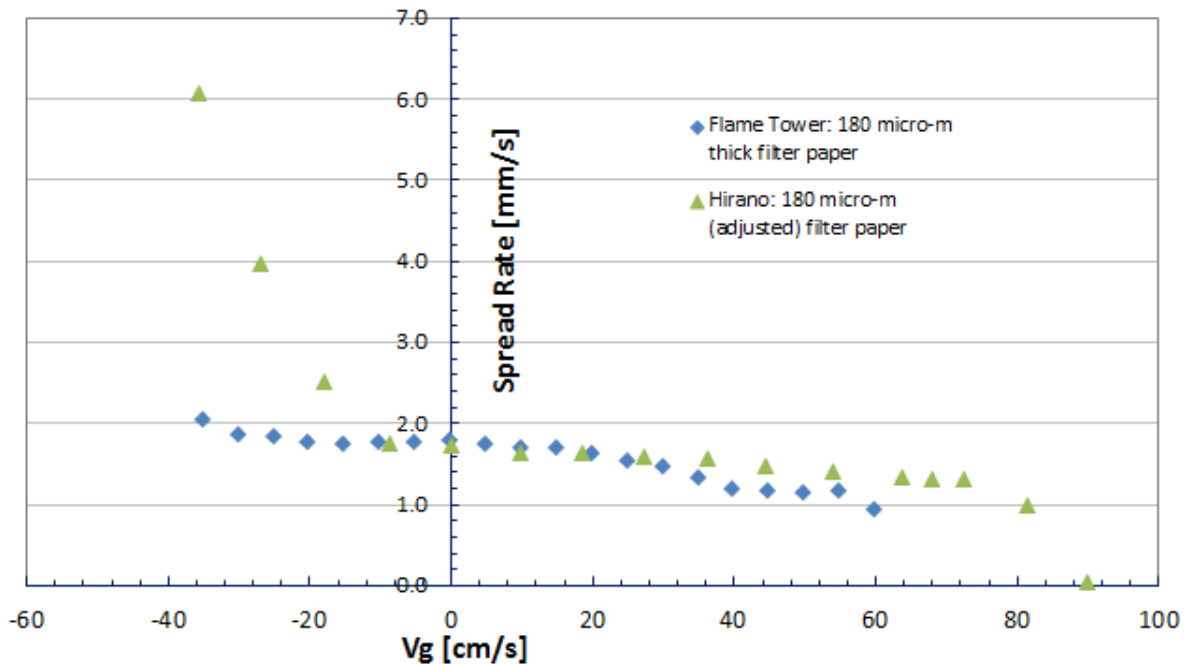


Fig. 23 Comparison of flame tower data with data from Hirano [29] obtained under similar conditions for a fuel thickness of 200 μm , which is adjusted in this plot to 180 μm by multiplying Hirano's spread rate with a factor 10/9.

The only work in literature that spans the flow velocity from the positive to negative side is due to Hirano et al. [29] who used a vertical wind tunnel. Although the data agree for

small values of V_g , the same is not true for the blow off extinction velocity or the concurrent flow flame spread rate. An examination of the flow configuration of the wind tunnel reveals that the boundary conditions are not symmetric when the flow is reversed, but more work is necessary to understand the discrepancy between these two sets of data.

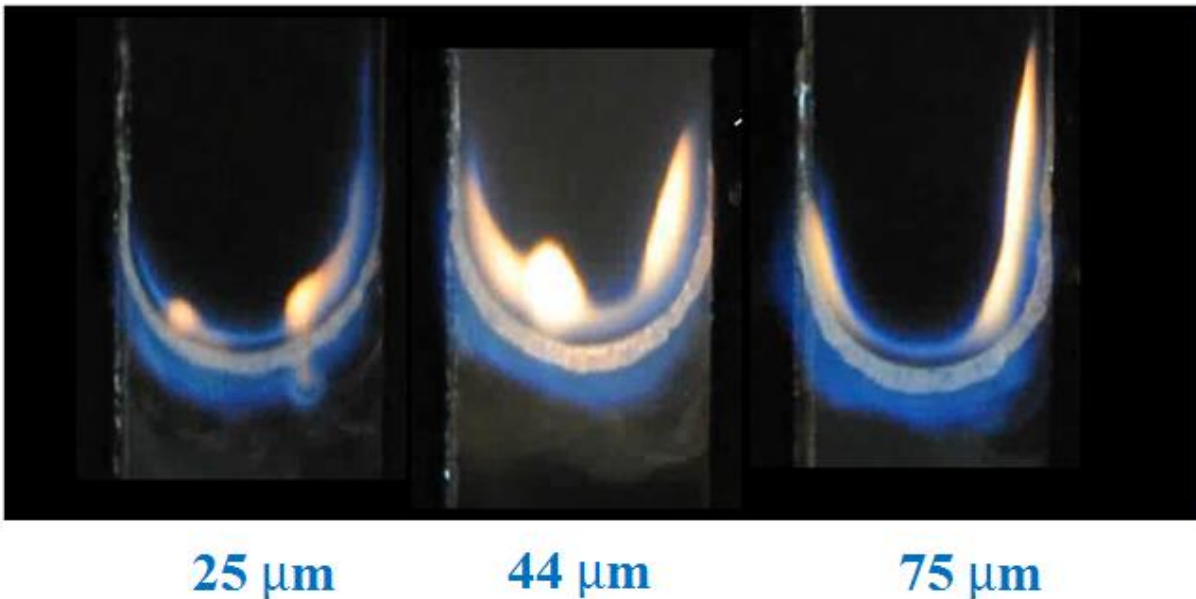


Fig. 24 Flame shapes for downward flame spread in ambient conditions over PMMA of three different thicknesses. The sample width is 3 cm for each case.

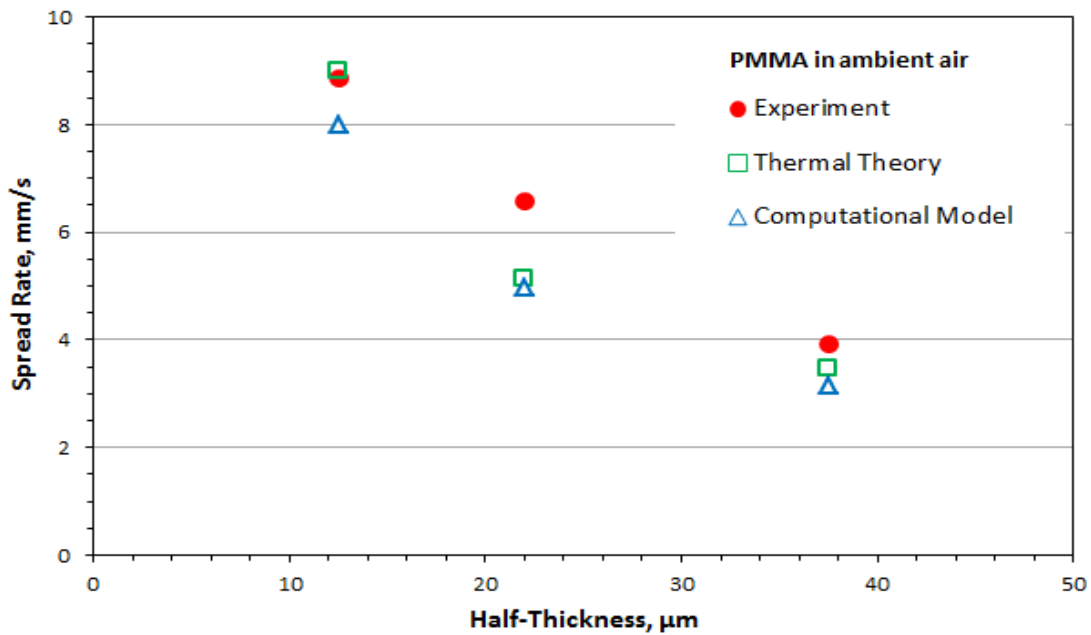


Fig. 25 Measured, computed, and theoretical [35] spread rate for the flames shown in Fig. 24..

2.4 Validation of Numerical Model

Downward flame spread experiments were conducted over 3 different thicknesses of PMMA sheets and ashless filter papers in ambient quiescent conditions and the spread rates and flame shapes are compared with the prediction of the numerical model described in Sec. 2.2. The PMMA flames, shown in Fig. 24, do not show any significant change in the visible flame image. The same conclusion can be reached from the computational flame images. The spread rates from the experiments are plotted along with the numerical results, and flame spread formulas

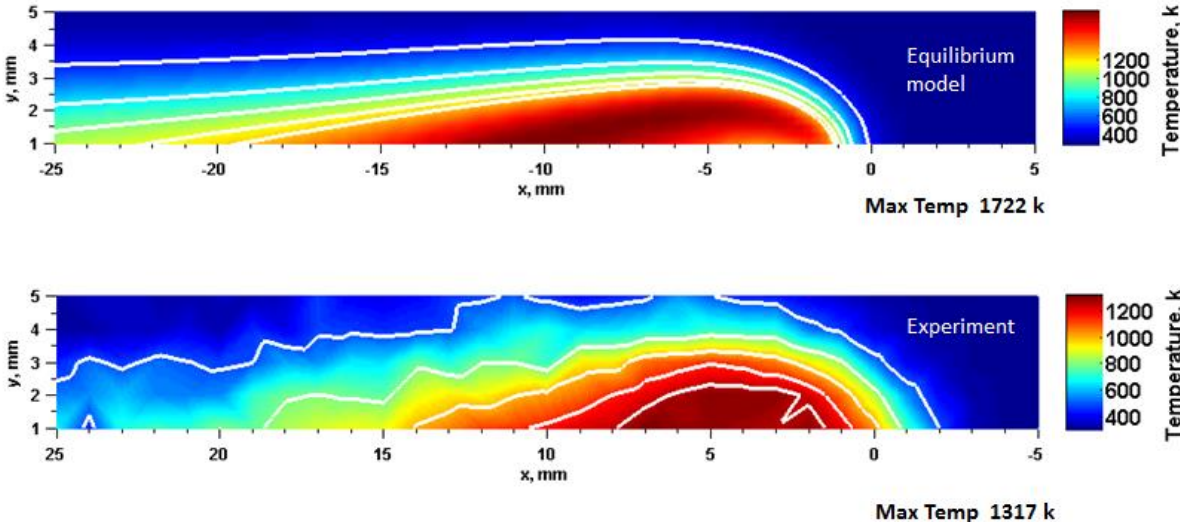


Fig. 26 Temperature field measurement of Fig. 14 is compared with computational prediction. The flame shapes agree remarkably well.

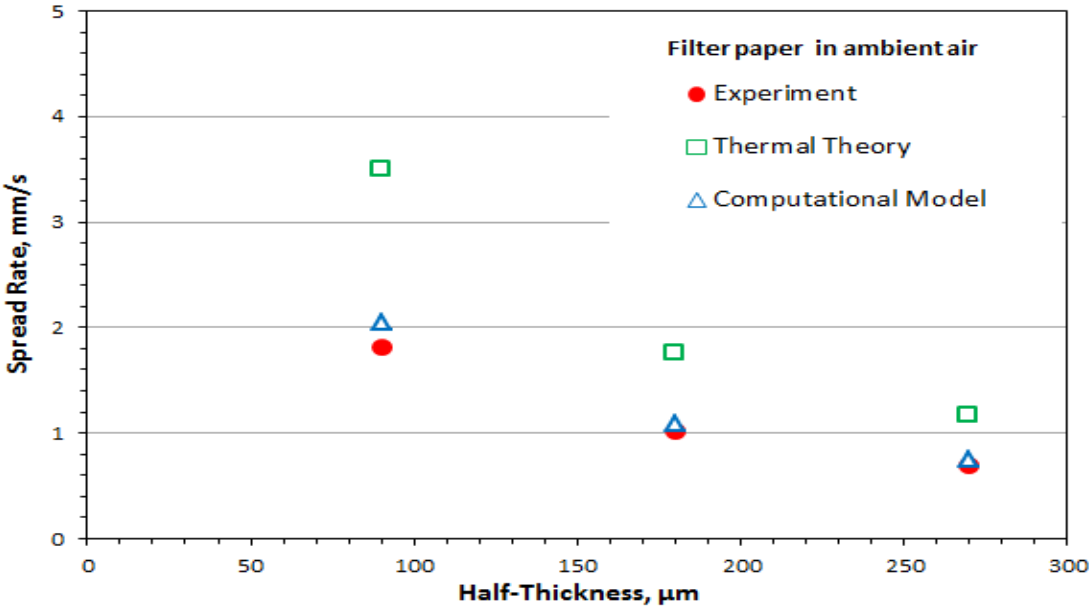


Fig. 27 Measured, computed, and theoretical [35] spread rate for downward flame spread over ashless filter paper of different thicknesses under ambient conditions.

from a modified thermal theory [35] which is implemented as a Java applet and accessible over the Internet [36] in Fig. 25. There seems to be reasonable agreement, and particularly good agreement between computational results and the thermal theory.

For flame spread over ashless filter paper, the temperature field measurement are compared with computational results in Fig. 26 which displays remarkable agreement in flame height and flame length. The temperature contours also look quite similar between the computations and experiments. It should be mentioned that the temperature measured by the 75 μm K type thermocouple is uncorrected for heat losses and other sources of uncertainties, which may explain the large difference between the maximum temperature measured, 1317 K, with the maximum computational temperature, 1722 K. The equilibrium temperature for cellulose burning in atmospheric air is calculated from the equilibrium RIA [34] as 2216 K. The difference between the computational and the equilibrium temperature can be attributed to radiative losses included in the numerical model.

3. FLIGHT EXPERIMENT

3.1 Project Goal

In previous NASA-funded flight experiments flame spread over thin ashless filter and thick PMMA in a quiescent environment were studied under different oxidizer conditions. The results showed that the flame speeded vigorously over thin ashless filter paper while gradually slowing down over. Computational modeling qualitatively explained this behavior and a theory was developed later that yielded spread rate formulas for both thin and thick fuels in a microgravity environment. One of the intriguing aspect of the theoretical prediction is that steady spread is impossible in a quiescent environment if the fuel thickness exceeds a certain critical value. The goal of the current project is threefold:

1. Determine if a spreading flame becomes unsteady if the fuel thickness exceeds a certain value.
2. Determine if the unsteady flame propagation leads to flame extinguishment.
3. Determine the mechanism of flame extinguishment.

To achieve these goals new experiments are required where a spreading flame can be observed over long duration over fuel samples of different thicknesses in a microgravity environment. Only ISS can provide such long duration platform for such experiments. Computation and theoretical results indicate that radiative losses is responsible for triggering this unsteady behavior. The non-dimensional number that controls the radiative losses in the governing equations is proportional to fuel thickness and inversely proportional to pressure. Therefore, we plan to vary pressure along with fuel thickness in these experiments. Computational results indicate that a separation between the temperature and products field in the gas phase is a possible pathway to flame extinguishment. To achieve Goal 3, temperature and carbon dioxide concentration measurement in the gas phase will provide valuable data to refine

the existing computational model. The spread rate data will help validate and improve the current closed-form flame spread formula. The critical thickness predicted by the theory and computation differ significantly and the experimental results will help identify the weakness in our theoretical models.

Understanding flame spread behavior has direct implications to fire safety and flame spread in a microgravity environment is completely different from that in normal gravity. This is because the absence of an opposing flow can make the residence time (time spent by oxidizer and fuel at the flame leading edge) relatively large ushering in strong radiative effects which are insignificant in the corresponding normal gravity flames due to high buoyant velocity. The possibility of establishing a critical fuel thickness formula, backed up by experiment, that predicts if a steady flame is possible or not has direct relevance to the fire safety goals of manned space missions.

3.2 Knowledge Lacking

Although computational and theoretical results indicate that a flame may extinguish for a fuel exceeding certain thickness in a quiescent microgravity environment, it is yet to be experimentally verified. Spread rate predicted by Eq. (16) for flame spread over PMMA in a 50-

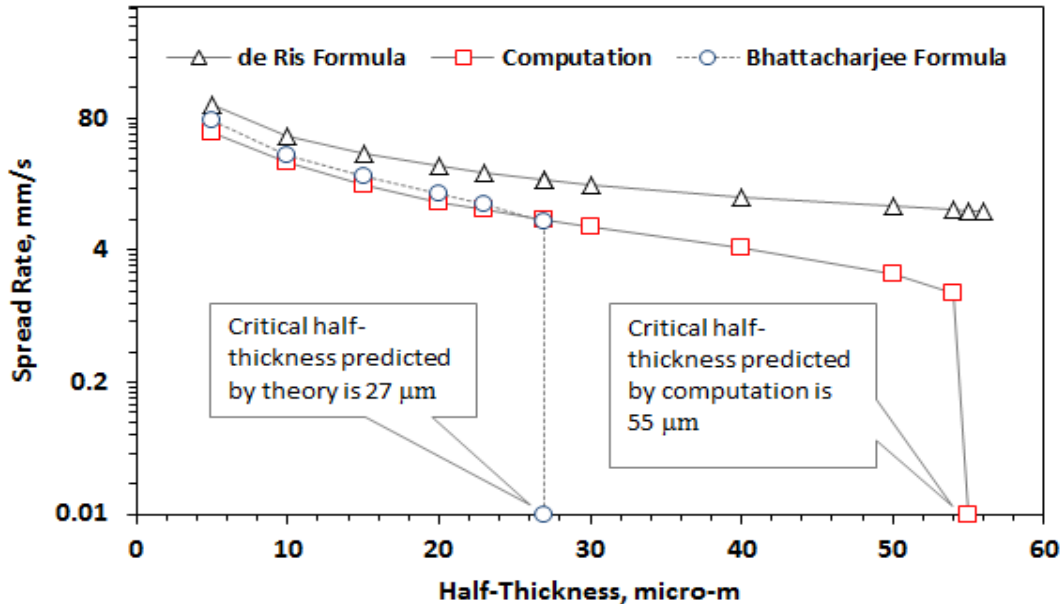


Fig. 28 Comparison of flame spread rate as a function of fuel half-thickness for flame spread over PMMA sheets at a 50-50 mixture of O₂/N₂ at 100 kPa. Computation and prediction from Eq. (15) indicates flames extinguishes after a certain critical thickness.

50 mixture (by volume) of oxygen and nitrogen at a total pressure of 100 kPa is plotted in Fig. 28

as a function of fuel thickness and compared with computational results from the validated numerical model and the de Ris formula [16] in the thermal regime. Evaluation of spread rate using Eq. (17) or de Ris formula [16] requires specification of fuel and oxidizer conditions along with thermodynamic and transport properties. To make the calculation of spread rate available to the community, it is implemented as a Java applet [37] accessible through the Internet. While the de Ris formula shows inverse-proportional relationship between the spread rate and fuel thickness, both computation and Eq. (18) predicts flame extinguishment after a certain half-thickness, $27\mu\text{m}$ from the formula and $55\mu\text{m}$ from computation. As can be seen from Eq. (8), \mathfrak{R}_0 , the non-dimensional radiation loss number is proportional to fuel half-thickness τ . As τ is increased, \mathfrak{R}_0 increases leading to a complex value for spread rate in Eq. (13), which is

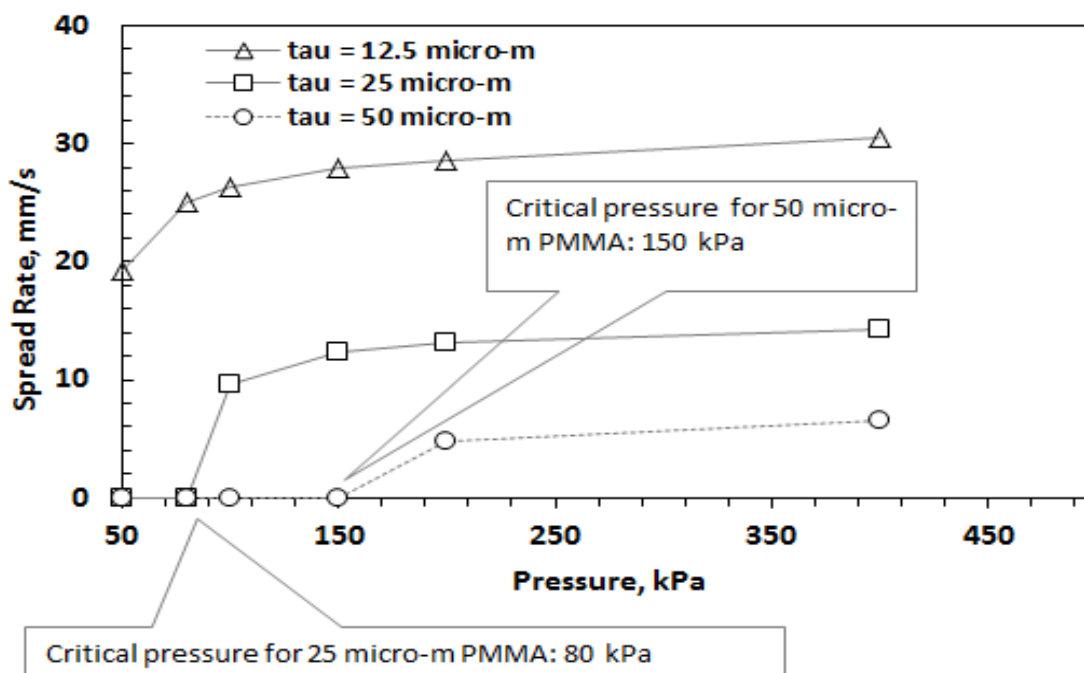


Fig. 29 Spread rate predicted by Eq. (19) as a function of total pressure for flame spread over PMMA sheets in a 50-50 mixture of O₂/N₂ at 100 kPa for three different thicknesses.

interpreted as flame extinguishment. But these are just predictions, never experimentally verified. Even establishing that a critical thickness exists will have a significant contribution to our understanding of microgravity flame spread.

From Eq. (8) it can also be seen that \mathfrak{R}_0 is inversely proportional to ρ_g , the density of the oxidizer, and hence must vary in direct proportion of the total pressure of oxidizer (by the use of ideal gas equation of state). For a given fuel thickness, a reduction of total pressure, therefore, is expected to reduce the flame spread rate leading to extinguishment. Spread rate predicted by Eq. (20) is plotted for three different thicknesses as a function of total pressure in Fig. 29. From

this plot, the critical pressure for the 25 μm half-thickness can be seen to be 80 kPa. This means below 80 kPa, steady spread rate cannot be sustained over this fuel. Does lowering the total pressure and or increasing the fuel thickness make inhibits vigorous flame spread? This is one of

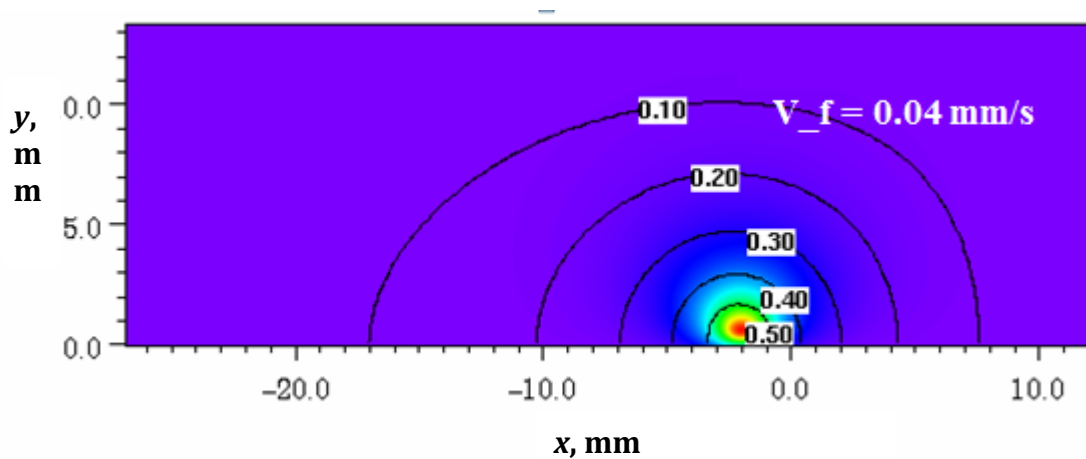


Fig. 30 Gas phase temperature field image and products mole fraction contours for flame spread over a 75 μm thick PMMA fuel in a 50-50 oxygen-nitrogen environment.

the questions we will seek answer to in the flight experiment.

As the fuel thickness is increased or the total pressure reduced, the flame spread rate gradually decreases. The temperature and oxygen concentration fields for a particular simulation is shown in Fig. 30, which shows that the products species diffuse further than the temperature field, whose size is restricted by the radiative losses. It is this asymmetry, according to computational results, that is at the heart of flame extinguishment. Currently there is no experimental data to confirm or refute this prediction.

3.3 Experimental Objectives

In order to test the proposed theory and refine the computational model, data from long duration microgravity experiments is necessary. The specific objectives of the flight experiments are:

1. Establish that steady flame spread over solid fuel in a quiescent microgravity environment is possible only if the fuel thickness is less than a critical value.
2. Investigate the propagation of the products and temperature field to uncover the mechanism of flame extinguishment.
3. Characterize how the ambient pressure and presence of a mild opposing flow affect the flame spread rate and extinction behavior.

3.4 Summary of Experimental Approach

3.4.1 Fuel and Oxidizer Conditions

We propose to study flame spread over PMMA (poly-methyl metacrylate) sheets of different thicknesses in a 50-50 mixture of oxygen and nitrogen. The selection of PMMA over filter paper, the two most well studied solid fuels, is predicated by the fact that thickness can be more easily altered (or available) for PMMA than cellulose. The elevated oxygen level, significantly above the LOI (low oxygen index), is meant to eliminate any possibility of oxygen limited extinguishment, leaving radiative losses as the only remaining mechanism of extinction in a quiescent environment.

We would like to use fuel samples of size 120 mm by 20 mm with six different fuel thicknesses: 25 μm , 50 μm , 100 μm , 250 μm , 1 mm, and 2 mm. The sample width is large enough to provide a two dimensional flame while small enough to prevent excessive oxygen consumption. The same logic is used to limit the length of the sample to 120 mm although we would prefer even longer sample if possible. Although the predicted critical thickness is about 100 μm , the larger thicknesses are included to provide data on time on extinction. Although not part of the main objectives, data on time of extinction will provide additional insight into the mechanism of flame extinguishment (Objective 2).

Ideally all the six samples will be loaded for a given ambient conditions all at once (using a carousel or cartridge). The samples will be burned one at a time for a given pressure of 100 kPa. The experiment will be repeated for a total pressure of 50 kPa with an identical set of samples.

3.4.2 Oxidizer Flow

Although the focus of our experiment is to get data for quiescent environment, a mild opposing flow for a certain initial period (TBD) will serve three purposes. First, the extra energy released by the ignition system will be convected away by the flow leaving the flame spread zone free of any after effect of ignition energy. Second, for thicker fuels presence of a flow will help establish a steady flame, absent which eventual flame extinguishment may be attributable to inadequate amount of ignition energy. Finally, the effect of a prescribed flow on flame propagation and extinguishment will provide additional data for expanding the scope of our analysis and further validating the computational results. The mild flow can be anywhere between 20 mm/s to 100 mm/s at the leading edge of the fuel.

3.4.3 Diagnostics

3.4.3.1 Color Imaging

At least two color CCD cameras will be used, one for the side view and one for the top view of the flame spread. The top view will be used for measuring the flame spread rate and must have the highest possible resolution (about 10 pixels per mm). The side view will be used to characterize the flame shape, size, and the stand-off distance and for real time downlink to monitor ignition.

3.4.3.2 Thermocouple Array

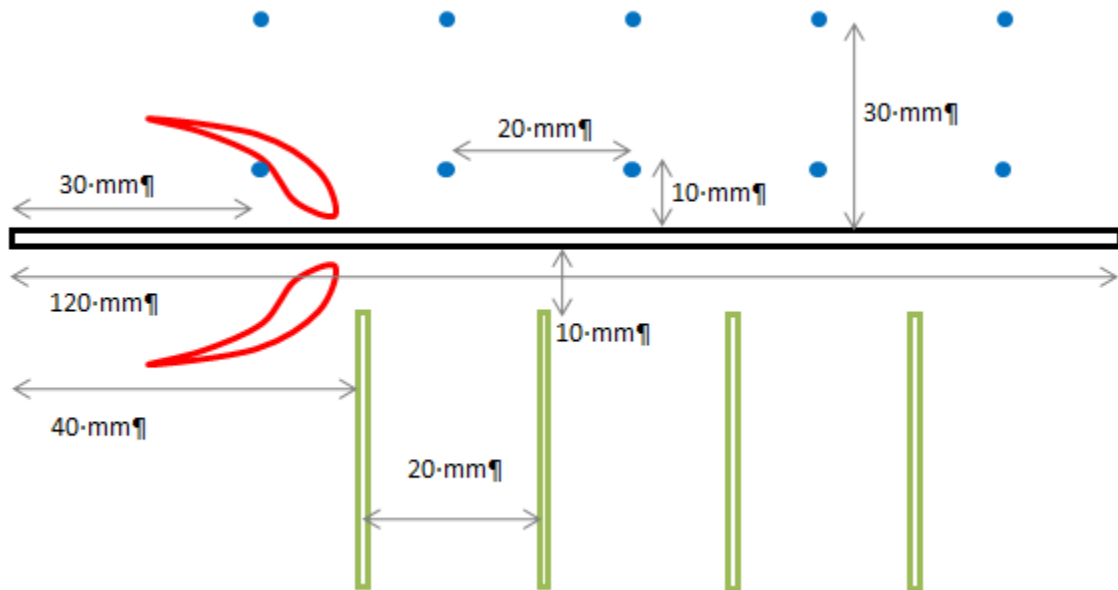


Fig. 31 Gas phase thermocouples and suction syringes for the CO₂ probes (exact locations and numbers TBD) will provide data to meet objective 2.

Two arrays of ten thermocouples as shown in Fig. 31 (precise position TBD) will be used to map the thermal image of the propagating flame as we have done for downward spreading flame in Fig. 14. The bead diameter should be as small as practically possible so as to reduce measurement error and, more importantly, affect the propagating flame in any significant manner.

3.4.3.3 Concentration Probe

At least two (and preferably four) CO₂ sensors will be used to measure the propagation speed of the products field. We have used an infra red sensor (see Fig. 32) for the downward flame experiments without any particular difficulty and measured CO₂ levels of up to 10% (by volume). Using hypodermic needle it may be possible to draw products from 10 mm away from the surface without disturbing the flame. Passing the gas through a desiccant can cool down the products and remove the

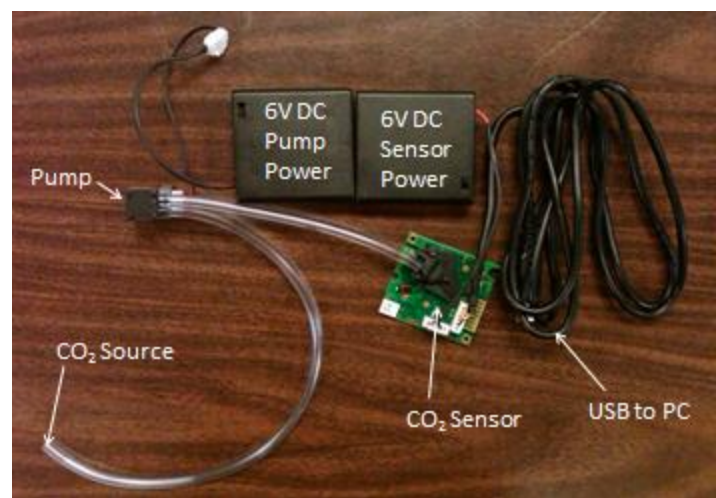


Fig. 32 The infrared CO₂ sensor and pump arrangement used to measure CO₂ concentration.

water vapor that is present in the products.

An oxygen sensor will be used to monitor the overall oxygen level in the chamber before and after the flame spread to ascertain that the oxygen concentration is not altered significantly because of the combustion of the earlier samples of PMMA. After each sample is burned, sufficient time will be allowed before the next sample is ignited so as to ensure complete diffusion of the products field. The measurements will be continued during that time to provide valuable data to test and improve the species transport sub-model of the computational model.

3.5 Science Data End Products and Requirements

Objective & Sub-Objective	SDEP	Requirement (RTDSF)
<p>Objective 1 Establish that steady flame spread over solid fuel in a quiescent microgravity environment is possible only if the fuel thickness is less than a critical value.</p> <p>Sub-Objective: 1a. Prepare fuel samples for ignition.</p>	<p>1. Plots of flame location as a function of time for different fuel thickness for a given environmental conditions.</p> <p>2.. Plot of flame size (length, height, and total visible area) as a function of time to monitor flame unsteadiness.</p>	<ol style="list-style-type: none"> 1. Prepare PMMA fuel samples of size 120 mm x 20 mm with thicknesses 25 μm, 50 μm, 100 μm, 250 μm, 1 mm, and 2 mm. Thickness tolerance: +- 5% as long as the final thickness is uniform and measured within 99% accuracy. Tolerance for exposed width and length: 1%. At SDSU we purchased 3 mil PMMA sheets and cemented them (with liquid acrylic cement) to make thicker sample. 2. Sample holder specification: low thermal conductivity material to avoid heat losses, small thickness to avoid heat losses and maximize side view of the flame, narrow width to minimize overall sample holder mass. 3. For a given ambient condition , all six different thicknesses should be burned one after another. The change in oxygen if all the fuel burns has been calculated to be within acceptable range. Altogether twelve samples will be burned in batches of six. If that is impractical, the twelve samples can be divided into three batches. 4. A ruler should be attached (on printed on) to the sample holder so that the flame location can be independently confirmed from the top – view camera. It will also allow variable

		<p>calibration (pixels/mm) if necessary.</p> <ol style="list-style-type: none"> An LED stopwatch that displays the data acquisition clock should be positioned in the camera view to synchronize captured video with sensor data. Clear area around the fuel except for sensors. Igniter should be at one end (away from the source of flow) and use minimum amount of energy (which should be recorded). After ignition, igniter does not have to be retracted.
<p>Sub-Objective: 1b Prepare the oxidizing environment.</p>	<ol style="list-style-type: none"> Plots of velocity profile at the leading edge of the fuel sample. Measurement of oxygen concentration and pressure inside the chamber 	<ol style="list-style-type: none"> Establish a 50-50 oxygen nitrogen (by volume) mixture at a total pressure of 100 kPa. Tolerance for the oxygen level and total pressure is 0.1%. Establish a mild external opposed flow of velocity, about 20 mm/s, during ignition. The direction of the flow should be opposite to the direction of flame spread. The velocity upstream of the sample should be known with in 1% accuracy. The external flow should be uniform (tolerance 5%) within a distance of at least 20 mm from the fuel surface. The flow must be turned off after a predetermined time or when the flame reaches the first thermocouple as indicated by a certain rise in its temperature. The purpose of the flow is to ensure that a spread is established, especially for thicker samples.
<p>Objective 2 Investigate the propagation of the products and temperature field to uncover the mechanism of flame</p>	<ol style="list-style-type: none"> Plots of temperature and concentration sensor data synchronized with the pyrolysis front location. Color top-view 	<ol style="list-style-type: none"> As the flame spreads, the pyrolysis front will be used to locate the flame. For that a top view of the flame spread must be captured using a CCD camera. The camera should produce at least 10 pixel per mm resolution, which translates to about 1000 pixels for the 100 mm long sample. The field of view of the camera should be about

<p>extinguishment.</p> <p>Sub-Objective: 2a Prepare the diagnostic sensors and cameras.</p>	<p>and color (and IR, if possible) side view of the flame showing the growth and possible decay of the flame leading to extinction.</p>	<p>100 mm x 30 mm with the centerline aligned with the axis of the fuel sample.</p> <ol style="list-style-type: none"> 2. As the flame spreads, the propagation of the thermal field will be monitored by two arrays of thermocouples located 10 mm and 30 mm away from the surface. Each array will have four gas phase thermocouples at x locations: 30 mm, 50 mm, 70 mm, 90 mm, and 110 mm (the ignition end being the origin). 3. The thermocouple size should be as small as possible to reduce effect on the spreading flame. One suggested way is to string the thermocouple parallel to the fuel surface, which reduces the conduction through the leads due to lower temperature gradient. 4. The propagation of the products field will be monitored by two CO₂ sensors (non GC continuous signal) in the gas phase, located x=50 mm and 100 mm, 30 mm away from the surface. The suction flow and the suction tube diameter must be minimized to reduce the impact of the flow on the flame spread. The suction tube also should have the least thermal mass so as not to act as a heat sink to the flame. Tolerance of mole fraction measured is 1%. 5. An oxygen sensor at a distance 50 mm from the surface, at x = 60 mm should monitor the oxygen level. Tolerance of mole fraction measured is 1%. 6. An IR camera should capture the side view of the flame propagation to track the propagation of the emissive field (a function of the gas temperature and the partial pressure of the radiating species, mostly CO₂ and H₂O). 7. An LED stopwatch that displays the data
--	---	---

		<p>acquisition clock should be positioned in the camera view to synchronize captured video with sensor data.</p> <p>8. Allow data acquisition to continue for a predetermined (TBD) amount of time or the signal from the oxygen sensor s showing no change.</p>
<p>Objective 3 Characterize how the ambient pressure and presence of a mild opposing flow affect the flame spread rate and extinction behavior.</p> <p>Sub-Objective: 3a Characterize the effect of ambient pressure on the flame spread process.</p>	<p>Plots and data produced as part of objectives 1 and 2 are repeated at a lower ambient pressure in which the radiative effects are expected to be amplified.</p>	<ol style="list-style-type: none"> 1. Change the chamber pressure to 50 kPa. Tolerance 1%. 2. Repeat the experiment for the same six fuel thicknesses 25 μm, 50 μm, 100 μm, 250 μm, 1 mm, and 2 mm..
<p>Sub-Objective: 3b Characterize the effect of the presence of an opposing flow.</p>	<p>No additional plots are required as data with flow velocity are already part of the overall data in each spread.</p>	<ol style="list-style-type: none"> 1. Each flame spread experiment starts with a mild forced opposing flow velocity (20 mm/s). 2. We will follow a multi-tiered approach to turn off the flow. If the experiment can be monitored in real time than the flow cut off time will be manually controlled (based on data from previous experiment) from the ground. If that does not work out, when the first thermocouple signal reaches a threshold, the flow will be cut off. If that fails, a pre-determined maximum time of flow will be used

		<p>as the fail-safe alternative.</p> <p>3. The change in flame shape and size as well as the flame spread rate when the flow is turned off will be captured by the CCD and IR camera as already explained.</p>
--	--	--

- [2] S. Bhattacharjee and R. A. Altenkirch, "Radiation-controlled, opposed-flow flame spread in a microgravity environment," in *Symposium (International) on Combustion*, Orleans, France (1991) 1627-1633.
- [3] Chiun—hsun Chen and Ming—Chou Cheng, "Gas-Phase Radiative Effects on Downward Flame Spread in Low Gravity," *Combustion Science and Technology* 97 (1) (1994) 63–83.
- [4] R. A. Altenkirch. NASA Solid Surface Combustion Experiments. [Online]. <http://microgravity.grc.nasa.gov/fcarchive/combustion/combust.htm>
- [5] R. A. Altenkirch, L. Tang, K. Sacksteder, S. Bhattacharjee, and A. Delichatsios, "Inherently Unsteady Flame Spread to Extinction over Thick Fuels in Microgravity," in *Twenty-Seventh (International) Symposium on Combustion, The Combustion Institute* (1998).
- [6] J. S. T'ien, "Diffusion flame extinction at small stretch rates: the mechanism of radiative loss," *Combustion and Flame* 65 (1986) 31-34.
- [7] S.L. Olson, P.V. Ferkul, and J.S. T'ien, "Upward flame spread over thin solids in partial gravity," *Proceedings of the Combustion Institute* 29 (2) (1988) 2569-2577.
- [8] S. Bhattacharjee, K. Wakai, and S. Takahashi, "Dynamics of Flame Spread in Microgravity," NASA, NASA Research Grant NRA99 2000-2004.
- [9] S.L. Olson, T. Kashiwagi, O. Fujita, M. Kikuchi, and K. Ito, *Journal of Heat Transfer* (1996) 118: 181.
- [10] F.A. Williams, in *Proceedings of the Combustion Institute* (1976) 16:1281–1294.
- [11] I.S. Wichman, *Prog. Energy Combust. Sci.* 18 (1992) 646-651.
- [12] I.S. Wichman and F.A. Williams, "A simplified model of flame spread in an opposed flow along a flat surface of a semi-infinite solid," *Combustion Science and Technology* 32 (1983) 91-125.
- [13] M.A. Delichatsios, in *Proceedings of the Combustion Institute* (1996) 26:1281.
- [14] Y. Chen and M. A. Delichatsios, "Creeping flame spread: Some new results and interpretation," *Combustion and Flame* 99 (1994) 601-609.
- [15] J. West, M. King, S. Bhattacharjee, and R. A. Altenkirch, "Heat Transfer Pathways in Flame Spreading Over Thick Fuels as a Function of the Flame Spread Regime: Microgravity, Thermal, and Kinetic," *Combustion Science and Technology* 127 (1997) 119-140.
- [16] J. N. de Ris, "Spread of a laminar diffusion flame," in *Symposium (International) on Combustion* 12 (1969) 24–252.
- [17] M. A. Delichatsios, "Exact Solution for the Rate of Creeping Flame Spread over Thermally Thin Materials," *Combustion Science and Technology* 44 (1986) 257.
- [18] S. Bhattacharjee and R. A. Altenkirch, "A comparison of theoretical and experimental results in flame spread over thin condensed fuels in a quiescent, microgravity environment," in *Symposium (International) on Combustion* 24 (1992) 1669-1676.
- [19] S. Bhattacharjee and R. A. Altenkirch, "Radiation-controlled, opposed-flow flame spread in a microgravity environment," 23 (1991) 1627-1633.

- [20] A. Kumar, K. Tolejko, and J. S. T'ien, "A Computation Study on Flame Radiation-Surface Interaction in Flame Spread Over Thin Solid-Fuel," in *The 6th ASME-JSME Thermal Engineering Joint Conference* (March 16-20, 2003).
- [21] Y. Son and P. D. Ronney, "Radiation-driven flame spread over thermally thick fuels in quiescent microgravity environments," in *Proceedings of the Combustion Institute* 29 (2002) 2587-2594.
- [22] S. Takahashi, M. Kondou, K. A. Wakai, and S. Bhattacharjee, "Effect of Radiation Loss on Flame Spread over a Thin PMMA Sheet in Microgravity," in *Proceedings of the Combustion Institute* 29 (2002).
- [23] R.A. Altenkirch, S. Olson, and S. Bhattacharjee, "Diffusive and Radiative Transport in Fires," NASA, NASA Contract NCC3-221 1993-1998.
- [24] S. Bhattacharjee, M. Bundy, C. Paolini, G. Patel, and W Tran, "A Novel Apparatus for Flame Spread Study," *Proceedings of the Combustion Institute* 34 (2012).
- [25] S.V., Patankar, "Numerical Heat Transfer and Fluid Flow," (1980).
- [26] S. Bhattacharjee, R. Ayala, K. Wakai, and S. Takahashi, "Opposed-Flow Flame Spread in Microgravity – Theoretical Prediction of Spread Rate and Flammability Maps," *Proceedings of the Combustion Institute* 30 (2004).
- [27] C. P. Paolini and S. Bhattacharjee, "A Web Service Infrastructure for Distributed Chemical Equilibrium Computation," in *Proceedings of the 6th International Conference on Computational Heat and Mass Transfer (ICCHMT)*, Guangzhou, China (2009).
- [28] C Paolini, S Bhattacharjee, W Tran, and F Miller, "A Novel Apparatus to Study Flame Spread at Low Concurrent or Opposed Flow Velocity," in *Joint Meeting of the Combustion Institute*, Park City, Utah (2013).
- [29] T.S. Hirano, S.E. Noreikis, and T.E. Waterman, "Measured velocity and temperature profiles near flames spreading over a thin combustible solid," *Combustion and Flame* 23 (1974) 83-96.
- [30] A.C. Fernandez-Pello and F.A. Williams, "Laminar Flame Spread over PMMA Surfaces," *Fifteenth Symposium (International) on Combustion*, The Combustion Institute, Pittsburgh, PA, (1975) 579.
- [31] A.C. Fernandez-Pello and R.J. Santoro, *Proc. Combust. Inst.* (1979) 1201-1209.
- [32] A. Ito and T. Kashiwagi, *Proc. Combust. Inst.* (1986) 65-74.
- [33] S. Bhattacharjee, J. West, and R.A. Altenkirch, "Determination of the Spread Rate in Opposed-Flow Flame Spread Over Thick Solid Fuels in the Thermal Regime," *Twenty-Sixth (International) Symposium on Combustion*, The Combustion Institute (1996) 1477-1485.
- [34] C. P. Paolini and S. Bhattacharjee, "A Web Service Infrastructure for Thermochemical Data," *J. Chem. Inf. Model.* 48 (7) (2008) 1511-1523.
- [35] S. Bhattacharjee, M. King, S. Takahashi, T. Nagumo, and K. A. Wakai, "Downward flame spread over poly(methyl)methacrylate," in *Symposium (International) on Combustion* 28 (2000) 2891-2897.
- [36] M. King and S Bhattacharjee. (2000) Java Applet for Downward Flame Spread Over Solid Fuels. [Online]. <http://sb.sdsu.edu/researchApps/downwardSpread/index.html>

- [37] S Bhattacharjee and R. Ayala. Java Applet for Flame Spread Calculations in the Microgravity Regime. [Online].
<http://sb.sdsu.edu/researchApps/microgSpread/index.html>
- [38] K. C. Lina, G. M. Faetha, P. B. Sunderlandb, D. L. Urbanb, and Z. G. Yuanb, "Shapes of nonbuoyant round luminous hydrocarbon/air laminar jet diffusion flames," *Combustion and Flame* 116 (3) (February 1999) 415-431.
- [39] Kumar Chittory, "An experimental approach to control buoyancy-induced flow in vertical flame spread over solid fuels," San Diego State University, San Diego, Thesis (M.S.) 2008.
- [40] Subrata Bhattacharjee, Richard Ayala, Kazunori Wakai, and Shuhei Takahashi, "Opposed-flow flame spread in microgravity-theoretical prediction of spread rate and flammability map," *Proceedings of the Combustion Institute* 30 (2) (January 2005) 2279-2286.
- [41] C. Paolini, K. H. Yeo, and S. Bhattacharjee, "An object oriented formulation for the finite volume simpler algorithm," in *Proceedings of the Western States Section/The Combustion Institute* (October 2003).
- [42] C. Paolini, K. H. Yeo, and S. Bhattacharjee, "An object oriented formulation for unsteady 3D heat transfer," in *Proceedings of CHT-04 ICHMT International Symposium on Advances in Computational Heat Transfer* (April 2004).
- [43] Jeffrey S. West, "Forced opposed flow flame spread over flat solid fuels in the thermal, near quiescent and chemical kinetic regimes," University of California, San Diego and San Diego State University, San Diego, Thesis (Ph. D.) 1998.
- [44] S. Bhattacharjee, K. A. Wakai, and S. Takahashi, "Prediction of a Critical Fuel Thickness for Flame Extinction in a Quiescent Microgravity Environment," *Combustion and Flame* 132 (3) (February 2003) 523-532.
- [45] Shuhei Takahashi, Manabu Kondou, Kazunori Wakai, and Subrata Bhattacharjee, "Effect of radiation loss on flame spread over a thin PMMA sheet in microgravity," in *Proceedings of the Combustion Institute* 29 (2002) 2579-2586.
- [46] C. Paolini, K. Bobba, P. Surana, and S. Bhattacharjee, "A Java Based Web Application for Performing Chemical Equilibrium Analysis in Thermodynamics Courses," in *36th ASEE/IEEE Frontiers in Education Conference*, San Diego, CA (October 28–31, 2006).
- [47] C. P. Paolini and S. Bhattacharjee, "An Object-Oriented Online Tool for Solving Generalized Chemical Equilibrium Problems," in *Proceedings of the 2008 ASME International Mechanical Engineering Congress and Exposition (IMECE08)*, Boston, Massachusetts (October 31 – November 6, 2008).
- [48] B. F. Webster, *Pitfalls of Object-Oriented Development.*, 1995.
- [49] S. Bhattacharjee, M. King, and C. Paolini, "Structure of Downward Spreading Flames: A Comparison of Numerical Simulation; Experimental Results and a Simplified Parabolic Theory," *Combustion Theory and Modeling* 8 (1) (March 2004) 23-39.
- [50] K. Wakai, K. Hanamura, S. Bhattacharjee, and S. Takahashi, "Flame-Spread Over Thin PMMA Under Micro-gravity Condition," Monbusho (Ministry of Education),

Grant-in-Aid for International Scientific Research 1999-2001.

- [51] A. Atreya, "Experimental and Theoretical Investigation of Heat and Mass Transfer Processes during Wood Pyrolysis," Univ. of Michigan, Michigan, 2009.
- [52] A.C. Fernandez-Pello, S.R. Ray, and I. Glassman, "Flame Spread in an Opposed Forced Flow: The Effect of Ambient Oxygen Concentration," in *Eighteenth Symposium (International) on Combustion*, Pittsburgh, PA 579.
- [53] A E Frey and J S T'ien, "A Theory of Flame Spread over a Solid Fuel Including Finite-Rate Chemical Kinetics," *Combustion and Flame* 36 (3) (1979) 263-289.
- [54] M D King, "A Simplified theory for Downward Flame Spread," San Diego State University, Thesis 1996.